JGR Oceans

RESEARCH ARTICLE
10.1029/2023JC019961

# Iron Limitation and Biogeochemical Effects in Southern California Current Coastal Upwelling Filaments

**K. O. Forsch[1], K. C. Fulton[1], M. M. Weiss[1], J. W. Krause[2,3], M. R. Stukel[4], and K. A. Barbeau[1]**

[1]Geosciences Research Division, Scripps Institution of Oceanography, University of California, San Diego, La Jolla, CA, USA, [2]Dauphin Island Sea Lab, Dauphin Island, AL, USA, [3]School of Marine & Environmental Sciences, University of South Alabama, Mobile, AL, USA, [4]Earth, Ocean, and Atmospheric Science Department, Florida State University, Tallahassee, FL, USA

**Key Points:**

- Upwelling filaments become Fe-limited features in the ocean, as sinking diatoms deplete surface dFe concentrations and are advected offshore
- Iron-limitation of diatom blooms is evidenced by in situ geochemical proxies (e.g., negative Siex) and deckboard Fe amendment experiments
- Greater biogenic silica-to-particulate organic carbon ratios among diatom communities make filaments hotspots of particulate matter export

**Supporting Information:**

Supporting Information may be found in the online version of this article.

**Correspondence to:**

K. O. Forsch,
kforsch@ucsd.edu

**Citation:**

Forsch, K. O., Fulton, K. C., Weiss, M. M., Krause, J. W., Stukel, M. R., & Barbeau, K. A. (2023). Iron limitation and biogeochemical effects in southern California Current coastal upwelling filaments. *Journal of Geophysical Research: Oceans*, *128*, e2023JC019961. https://doi.org/10.1029/2023JC019961

Received 21 APR 2023
Accepted 26 SEP 2023



**Abstract** In the spring and summer, high rates of primary production occur in the California Current Ecosystem (CCE) when nutrients are supplied to the euphotic zone. During periods of intense coastal upwelling, a flux of the micronutrient iron comes from nearshore sedimentary sources. In this upwelling region, mesoscale filament features distribute iron laterally, leading to distinct iron-influenced ecological zones. This study is the first to focus on the biogeochemical links between iron, the macronutrients, and particulates in coastal upwelling filaments. Broad spatial patterns of iron and biogenic silica concentrations, and proxies of iron-stress of diatoms, support results from microcosm amendment studies conducted during CCE Long Term Ecological Research process cruises in the summers of 2017 and 2019. We found that the benthic boundary layer and shoreward filament endmember supply dissolved and total dissolvable iron to this feature, but rapid assimilation and sinking by biogenic particles (e.g., diatoms) depletes the surface concentrations. Subsequently, diatom blooms which form in recently upwelled water masses become iron limited over time, thereby affecting the ratios of surface macronutrient reservoirs and biogeochemical advective fluxes. The development of Fe-limitation during lateral advection may lead to efficient carbon export downstream and offshore of the region with the highest phytoplankton growth rates and productivity.

**Plain Language Summary** Along the western continental margin of the United States, seasonal upwelling filaments appear as fast-flowing waters with high concentrations of nutrients (e.g., nitrate, silicic acid, iron) and phytoplankton. Diatoms dominate the phytoplankton communities in filaments, and they accumulate particulate matter as organic carbon and dense biogenic silica. During transport offshore, diatoms quickly deplete the surface of the critical micronutrient iron (Fe) and become Fe-limited. Using shipboard incubation experiments, we show that Fe-stressed diatom communities become more heavily silicified, and thus denser. Iron-stress indicators consistently correspond with these phytoplankton community biochemical reconfigurations in two separate studies of filaments, thereby demonstrating a mechanism for enhanced diatom community export out of the surface ocean in later stages of filaments.

## 1. Introduction

The California Current (CC) is the eastern limb of the large, clockwise circulation of the North Pacific Ocean subtropical gyre. The California Current Ecosystem (CCE) of central and southern California consists of a broad, eddy-rich, southward flowing section of the CC, a persistent but variable subsurface California Undercurrent (CUC) centered on the continental slope, carrying water from the tropics poleward, and an energetic and seasonally dynamic zone of frontogenesis and mixing near the continental shelf. This nearshore zone alternates between a wind-driven equatorward flow, driving periods of intense coastal upwelling in spring and summer, to a poleward flow in the fall and winter (Hickey, 1998).

Upwelling of cold, dense, nutrient-rich water occurs when equatorward winds strengthen during the summer through the process of Ekman transport. When this occurs in the CCE, which is a characteristic Eastern Boundary Upwelling System, high rates of primary production may be observed in these upwelled waters (Carr & Kearns, 2003; Checkley & Barth, 2009). Despite the small spatial area that Eastern Boundary Upwelling Systems occupy in the ocean (<1%), they host nearly 20% of global fisheries yield (Carr, 2001).

Macronutrient (e.g., nitrate $NO_3^-$, silicic acid $Si(OH)_4$, phosphate $PO_4^{3-}$) replete conditions in upwelled waters in the CC region, which typically have ~20% more silicic acid $Si(OH)_4$ than nitrate $NO_3^-$ (Zentara & Kamykowski, 1977),

generally result in blooms of diatoms (Van Oostende et al., 2015). Diatoms are an abundant type of phytoplankton that have an obligate requirement for silicon, which they use to make their siliceous shells (frustules). Due to their relatively large size and fast growth rates, they are critical components of oceanic primary production; globally, their carbon fixation rivals all terrestrial rain forests and they account for up to 40% of all marine carbon export (Field et al., 1998; Marchetti & Cassar, 2009; Nelson et al., 1995). Frustules offer some protection from zooplankton grazers (Wilken et al., 2011; Zhang et al., 2017) and impart mineral ballast to diatoms' organic material, making it more likely to sink from the surface layer. For these reasons, diatoms are major exporters of both Si and organic carbon from the euphotic zone (Smetacek, 1999; Timmermans et al., 2004). Factors that affect diatoms' nutrient uptake, growth, sinking rates, and remineralization rates can have major impacts on macro- and micronutrient cycling, coupling of pelagic and benthic communities, and carbon sequestration.

Iron (Fe) supply in upwelling regions is an important bottom-up control on diatom communities (Bruland et al., 2005; Hogle et al., 2018; Hutchins & Bruland, 1998; King and Barbeau, 2007, 2011). Studies indicate that new dissolved iron (dFe) sources to the ocean are rapidly removed from the water column (Boyle et al., 1977), which means that during blooms of diatom species with high cellular Fe quotas (Twining et al., 2021), the diatom community dFe demand will increase while supply decreases. Fe-limitation has been observed in high production, coastally-upwelled water masses in Eastern Boundary Upwelling Systems (Biller et al., 2013; Bruland et al., 2001; Firme et al., 2003; Hutchins & Bruland, 1998; Johnson et al., 1999; Till et al., 2019). Deckboard and in situ bottle-amendment experiments in many cases show a rapid response of the diatom community to the addition of dFe, indicating some degree of Fe-limitation.

Links between Fe and Si biogeochemistry are particularly important in areas of natural Fe-limitation. Low-latitude nutrient-replete marine diatoms use dissolved $NO_3^-$ and $Si(OH)_4$, on average, in approximately equimolar ratios, that is, 1:1 (Brzezinski, 1985). Under Fe-limitation and in the absence of significant kinetic limitation by suboptimal $Si(OH)_4$ concentration (which can reduce Si uptake and cellular quota), this uptake ratio is significantly altered (Hutchins & Bruland, 1998; Takeda, 1998), increasing to 4–6 (Franck et al., 2003), and thereby increases cellular Si content (De La Rocha et al., 2000). This has been documented in areas of natural Fe fertilization and in bottle manipulation experiments (Brzezinski et al., 2015; Hoffmann et al., 2007; Price, 2005; Takeda, 1998; Twining et al., 2004). Under Fe limiting conditions in systems with high $Si(OH)_4$, diatoms may preferentially deplete the surface reservoir of $Si(OH)_4$, relative to nitrate, and drive the occurrence of negative $Si_{ex}$ $\left(Si_{ex} = [Si(OH)_4] - R_{Si(OH)4:NO_3^-} \times [NO_3^-]\right)$ values in the water column. Indeed, negative $Si_{ex}$ values are co-located with subsurface Chla maxima in the CCE where there is direct evidence of Fe-limitation (Hogle et al., 2018).

Previous studies have demonstrated changes in diatom nutrient uptake ratios in response to Fe-limitation, and shown linkages between export efficiency and diatom Fe-limitation in the CCE (Brzezinski et al., 2015; Krause et al., 2015; Stukel et al., 2017). Episodic mesoscale features, such as eddies and filaments, can move upwelling-related Fe fertilization events offshore. As upwelling waters flow over the continental shelf, they become enriched in resuspended Fe-rich sediments (Bruland et al., 2001) and Fe-binding ligands accumulated from riverine input (Biller et al., 2013; Bundy et al., 2014; Homoky et al., 2012). These turbid layers overlying continental shelves are thought to be the primary source of new Fe (mainly as mineral Fe forms) for upwelling-associated blooms (Chase et al., 2005; Elrod et al., 2004; Johnson et al., 1999). Fluvial inputs accumulate in the benthic boundary layer (BBL) over the winter season and are transported to the surface with strong spring and summer upwelling. As upwelling water masses age and move offshore, there is a tendency for Fe limiting conditions to develop based on both direct assessment (King & Barbeau, 2007; Till et al., 2019) and molecular markers of Fe stress (Krause et al., 2020).

The data presented here follows the progression of two upwelling filaments, from recently upwelled and nutrient-replete to aged and Fe-limited conditions, to gain insight into the changing dynamics of Fe and biogenic silica (bSi, proxy for diatom biomass) as this evolution occurs. Filaments are characteristic of most eastern boundary currents (e.g., Chabert et al., 2021; Rossi et al., 2013; Sangrà et al., 2015) and usually contain a long core of cold water that originates from subsurface water upwelled near the coast. They have cross filament scales of 10–50 km, and along-filament scales of 50–200 km (Zaba et al., 2021). The offshore flows make filaments efficient vehicles for transporting biogeochemical tracers from zones of upwelling to offshore waters, with nutrient-rich conditions enabling the formation of phytoplankton blooms and fast-moving cores which advect particulate matter offshore (Gangrade & Franks, 2023; Mohrholz et al., 2014; Muller et al., 2013; Nagai et al., 2015). Mesoscale features such as filaments can contain a predictable primary producer population gradient

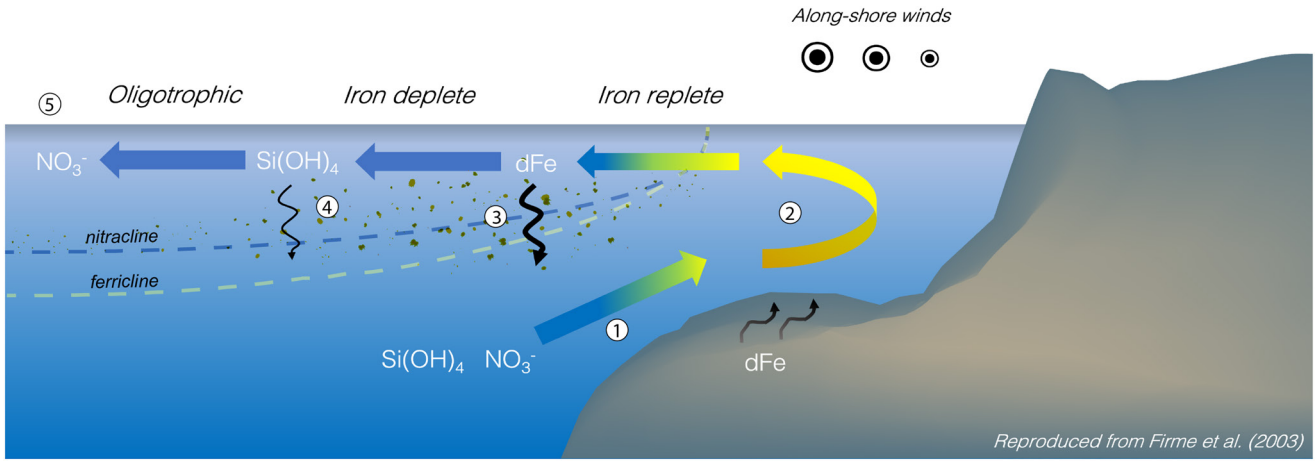


**Figure 1.** *Framework for the biogeochemical evolution of a coastal upwelling filament in the California Current Ecosystem*. During prolonged periods of intense along-shore winds, water masses on the continental slope, enriched in remineralized macronutrients ($Si(OH)_4$ and $NO_3^-$), are upwelled to the surface, replacing offshore-transported surface water near the coast ①. During episodes of wind-driven upwelling, deep water masses impinge on the shelf and interact with muddy continental shelf sediments. Resuspended Fe-bearing sediments from these muds form a turbid benthic boundary layer, which is entrained into the euphotic zone creating iron replete conditions for primary producers ②. This pulse of macro- and micronutrients selects for quickly-growing diatoms. The cold, nutrient-rich water parcel can be detected by autonomous and ship-towed instrumentation, as well as by remote detectors. The water parcel is inadequately mixed with the surrounding ocean and is advected offshore forming a filament. High rates of primary production and reduced losses (e.g., grazing, viral lysis) within the filament lead to the formation of a diatom bloom. When this occurs, Fe is preferentially removed from the surface layer (relative to $Si(OH)_4$ and $NO_3^-$) as sinking biogenic and mineral particles, leading to decoupling of the ferricline and nitracline ③. Once off the shelf, concentrations of Fe are heavily depleted and a relative excess of macronutrients (high $NO_3^-$:dFe ratio) results in Fe limitation of the diatom community. A lack of Fe inhibits key diatom metabolic processes, such as $NO_3^-$ assimilation and carbon fixation, but not precipitation of biogenic silica (bSi) frustules. Fe-limited diatoms preferentially deplete the surface $Si(OH)_4$ reservoir (relative to $NO_3^-$) and begin to senesce and sink ④. With the $Si(OH)_4$ reservoir depleted, the phytoplankton community shifts toward non-silicifying phytoplankton favored to better persist at the edge of the oligotrophic subtropical gyre, the furthest detectable trace of the filament ⑤. This figure was reproduced from Firme et al. (2003).

driven by processes of mixing, nutrient drawdown, and phytoplankton community evolution (e.g., diatom to dinoflagellate, Krause et al., 2020). Thus, they are excellent natural laboratories for studying processes of ecosystem connectivity and ecological transitions (Kranz et al., 2020; Wang et al., 2020). While filaments as physical phenomena and Fe-limitation as a biogeochemical condition have both been studied in the CCE for decades, no published work has yet examined these concepts simultaneously.

The study locations were chosen because of their characteristic seasonal filaments. The coastline north of the Point Conception region has multiple headlands and narrow continental shelves. In this region, cool pools often form (Sverdrup, 1938) and upwelled waters meet northward flowing coastal currents (Barth & Brink, 1987; Winant et al., 1999, 2003). Cold filaments can form and propagate 10 s of km offshore where they can be tracked for hundreds of km (Centurioni et al., 2008; Kim et al., 2011). We hypothesized that filaments would likely be particularly susceptible to the development of Fe-limitation as upwelling water picks up Fe from the BBL but is then rapidly transported offshore and away from the Fe sources; phytoplankton take up Fe through production or organic matter and their export of this material out of the euphotic zone removes it from the system. The framework we build upon is that as coastal filaments are drawn offshore, diatom communities become Fe limited, leading to preferential removal of Si as sinking biogenic material (Figure 1). We argue that changes in diatom physiology and community succession which are driven by the availability of dFe in coastal upwelling filaments may lead to enhanced carbon export and pelagic-deep ocean coupling in the CCE. Simultaneous assessments of the Fe geochemical condition and feature-tracked export of diatom-dominated blooms enabled us to systematically assess these properties in coastal upwelling filaments in the CCE.

This study addresses important aspects of Fe biogeochemistry in the CCE, with an emphasis on eastern boundary coastal upwelling filaments. We address the following questions: What is the source of iron to filaments? Are there distinct iron-influenced ecological regimes? What are the consequences of iron-limitation on the biogeochemistry of the macronutrients, bSi, and carbon?

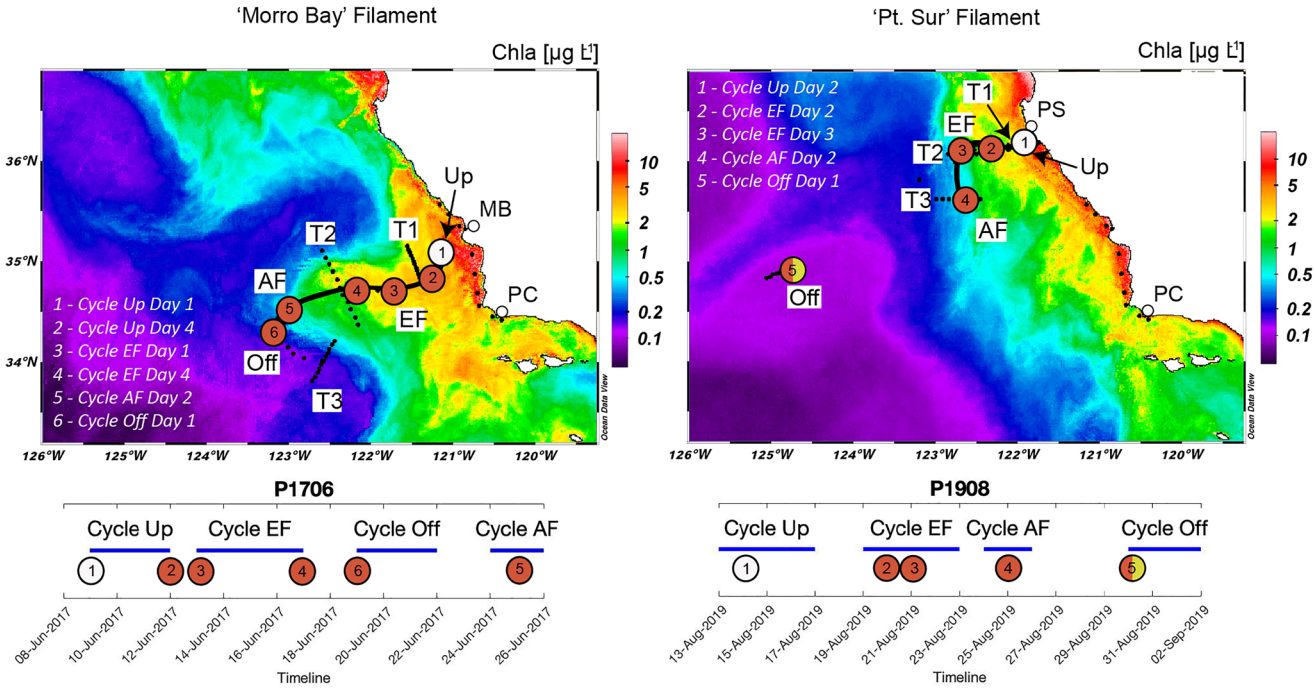


**Figure 2.** On-deck experiment locations during the "Morro Bay" (left) and "Pt. Sur" (right) filaments. Red circles indicate Fe-limited sites (as indicated by Chla and nitrate drawdown response in deck-board incubations). Split red-yellow symbol indicates Fe-$NO_3^-$ co-limitation. White symbol indicates no micronutrient limitation detected. Black line roughly indicates the filament track for the Lagrangian cycles. A timeline below each map shows the duration of cycles (blue horizontal bars) and the day on which deckboard incubation experiments were initialized. Chla data courtesy of Mati Kahru (Scripps Institution of Oceanography). Merged sensors used for Chla maps (http://spg-satdata.ucsd.edu/) are MODISA, MODIST, VIIRS-SNPP, OLCIA-WRR, and VIIRS-JPSS1 for "Morro Bay" filament (composite 9–25 June 2017) and additionally OLCIB-WRR and SGLI for "Pt. Sur" filament (composite 5 August to 3 September 2019).

## 2. Materials and Methods

### 2.1. Study Sites and Lagrangian Approach

An initial hydrographic survey was conducted using a towed SeaSoar and a ship-mounted Acoustic Doppler Current Profiler. In June 2017, a cold, chlorophyll-rich, and offshore-moving water parcel was detected in Morro Bay (MB) (Figure 2). Over the span of 2 weeks (9–25 June), the "Morro Bay" Filament (P1706, or MBF herein) was tracked aboard the *R/V Roger Revelle*. On the next process cruise in August 2019, another upwelled water parcel was identified just south of Pt. Sur (Figure 2). The "Pt. Sur" Filament (P1908, or PSF herein) was tracked aboard the *R/V Atlantis*. In the fashion of previous CCE process studies (Landry et al., 2009), four Lagrangian studies of each filament (termed cycles; Up = *upwelling*, EF = *early filament*, AF = *aged filament*, Off = *offshore CC*, herein) followed the upwelled water parcel by deploying low-profile (above freeboard) floating drift arrays and sediment traps, each equipped with a holey sock drogue centered at 15 m depth to catch mixed layer surface currents. Drifters were deployed at the beginning of each cycle, initiating a study period of 2–5 days per cycle. Locations for the beginning of each cycle were chosen based on Spray glider, remote sensing (Chla), and Moving Vessel Profiler survey data.

Cross-filament surveys were achieved by sampling in a line perpendicular to the mean current of the filament ("Transects"), capturing the structure and bounds of the filament over a 24 hr period. This sampling strategy allowed for quasi-synoptic portraits of the filament structure, important for the quantification of lateral biogeochemical fluxes. A BBL survey was conducted of the shoreward filament endmember at MB in 2017 (35.35°N, −120.93°E) and Pt. Sur in 2019 (36.23°N, −121.83°E) located on the inner-continental shelf. Additional sampling of long-term BBL transect sites and the Santa Barbara Basin station were conducted following the last filament cycle (30 June 2017, and 4 September 2019) as part of an ongoing timeseries.

### 2.2. In Situ Samples

During cycles and transects, profiles of macronutrients, bSi, Chla, and particulate organic carbon (POC) were generated from seawater samples collected from Niskin bottles daily (~11:00, local). Trace metal clean samples

for dFe and TDFe were sampled from Teflon-coated X-Niskin bottles on a powder-coated rosette, deployed on a coated hydrowire (Kevlar line). Fe samples were handled in a Class 100 trace metal clean van and filtered in-line using acid-washed Teflon tubing and acid-washed 0.2 µm Acropak-200 capsule filters pressurized by filtered air. Filtered samples were acidified to pH 1.8 with HCl (Optima Grade, VWR) and stored in 250 mL acid-clean low-density polyethylene bottles for on-shore analysis using flow-injection analysis with chemiluminescence (King & Barbeau, 2007). The trace metal methods described here are to the standards of the GEOTRACES program (Cutter & Bruland, 2012). Analyses of in situ samples and cleaning of sampling materials are detailed in Supporting Information S1.

### 2.3. Benthic Boundary Layer Sampling

Trace metal clean samples from the BBL were collected using Teflon-coated 10-L GO-Flo bottles (General Oceanics) suspended on a Kevlar line and triggered with Teflon messengers. Hydrographic data were collected using the ship's rosette system, which contained a conductivity, temperature, and depth (CTD) sensor as well as a fluorometer, dissolved oxygen (DO) sensor, and transmissometer. The BBL sampling locations were determined based on the local maximum in beam attenuation within 10 m of the ocean bottom obtained from a CTD cast immediately preceding the GO-Flo cast. An attempt was made to obtain the GO-Flo sample approximately five m off the bottom and within the BBL. Nine stations were sampled during the MBF. Three PSF BBL stations were sampled near the shoreward filament endmember within 5 km of the coast. An additional nine stations were sampled during the 2019 BBL transect, reoccupying stations sampled in 2017.

### 2.4. Fe Addition Grow-Out Incubations

The biochemical response of the phytoplankton community to the addition of Fe was tested in incubation studies. These were initialized during the Lagrangian cycles at various stages of each cruise. Seawater from the trace metal clean rosette was collected from the depth of maximum Chlorophyll-a (Chla) fluorescence and placed into acid-cleaned 2.7 L polycarbonate bottles with unamended controls and +Fe (5 nmol $L^{-1}$ $FeCl_3$ in pH 1.8 deionized water) treatment. Each treatment was done in triplicate. On-deck incubations were conducted in flow-through incubators (sea surface temperature) screened to 30% surface irradiance using nickel grating for 3–4 days. On-deck incubation studies were sampled daily for Chla and macronutrients ($NO_3^-$ and $Si(OH)_4$) while bSi, POC and community composition were sampled at the final timepoint ($t_f$). The water sampled from the rosette for these experiments was analyzed for dFe. For the MBF and PSF, the phytoplankton community composition was assessed by CHEMTAX analysis of major taxonomical pigment concentrations determined by high-performance liquid-chromatography of surface seawater. For PSF, the community composition was additionally assessed by 18S genomic sampling on the initial sample ($t_0$). During the PSF cruise, an additional two treatments (+N and +N/+Fe, using 10 µM $NO_3^-$ additions) were used in the PSF-Off incubation experiment to test for $NO_3^-$ and dFe co-limitation at the subsurface chlorophyll maximum and screened to ~9% of surface irradiance to represent low light levels found at depth.

### 2.5. Sediment Traps

VERTEX-style particle interceptor traps were placed on a sediment trap array at three nominal depths: 150, 100 m, and the base of the euphotic zone (40–60 m). Tubes contained a solution made from 0.1 µm filtered seawater amended with 60 g $L^{-1}$ NaCl and 0.4% (v/v, final concentration) formaldehyde. Sediment traps were deployed at the beginning of a cycle and collected on the last day of the cycle; thus, vertical flux was quantified over the entire cycle period (Knauer et al., 1979; Morrow et al., 2018). For the PSF, an additional deep trap was deployed at Cycles EF, AF, and Off at a nominal depth of 450 m.

## 3. Results

### 3.1. Spatial Orientation

#### 3.1.1. MBF (P1706)

Remotely sensed sea surface temperature and Chla, and MVP profiling transects informed the location for the first Lagrangian cycle. The water parcel was relatively low temperature (10–12°C), relatively high salinity (33.75

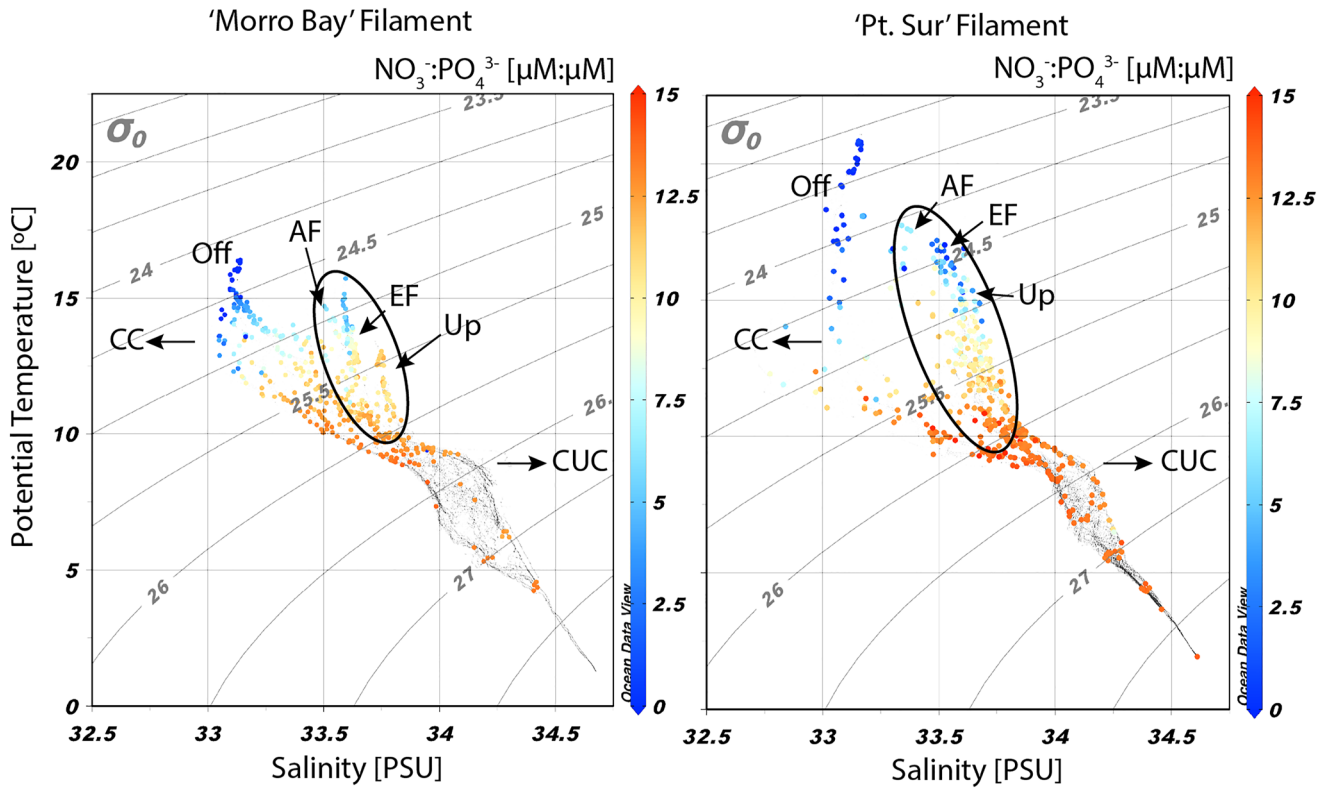


**Figure 3.** Potential Temperature versus Salinity ($\theta$-S) diagram of the "Morro Bay" (left) and "Pt. Sur" (right) filaments. The color bar is nitrate:phosphate ratio. The ellipse outlines the stations located within the surface filament core, distinguished by its relatively high salinity signature from upwelled California Undercurrent (CUC) water sources, compared to the relatively fresh and offshore California Current (CC) surface water (Zaba et al., 2021). Contours of constant potential ($\sigma_\theta$) density are overlaid. Based on the location of the CUC along CalCOFI line 93.30 according to Bograd et al. (2019), the $NO_3^-$:$PO_4^{3-}$ ratio at $\sigma_\theta = 25.8$ kg m$^{-3}$ was 11.73 and 12.20, in 2017 and 2019 respectively. The $NO_3^-$ : $PO_4^{3-}$ ratio at $\sigma_\theta = 26.5$ kg m$^{-3}$ was 11.06 and 11.51, in 2017 and 2019 respectively.

PSU), high in Chla (14.1 µg L$^{-1}$) and located on the shelf near MB with a fast-moving southwestward flow. Cycle MBF-EF began off the shelf and within the filament (Chla 3.8 µg L$^{-1}$), 71 km southwest from the start-point of Cycle MBF-Up. At the end of MBF-EF, a sediment trap drift array (Cycle MBF-EF.5) was deployed and left for 5 days while MBF-Off was completed, 135 km southwest of the start-point of MBF-EF (Figure 2). MBF-AF sampling was conducted at the location of the sediment trap array recovered at the end of MBF-EF.5, in the northeastward flow, the most time-evolved signature of the MBF (Chla 0.19 µg L$^{-1}$). A Potential Temperature versus Salinity ($\theta$-S) plot (Figure 3) shows that the signatures of the water masses in Cycles MBF-Up, EF, and AF have similar water mass origins while MBF-Off is heavily modified and did not resemble the filament. Besides the first day, MBF-Off was conducted in a relatively fresher water mass, more characteristic of CC water.

#### 3.1.2. PSF (P1908)

The PSF process study was initiated toward the end of the upwelling season (18 August to 2 September 2019). A pool of cold and salty upwelled water formed just south of PS and was quickly advected ~75 km offshore directly west (Cycles PSF-Up and PSF-EF), before warming significantly and moving 25 km south (Cycle PSF-AF, Figure 2). The Chla concentration within the filament began with 9.8 µg L$^{-1}$ in early cycles and decreased to 0.4 µg L$^{-1}$ by the end. Cycle PSF-Off was started in a westward propagating water mass characterized by well stratified, relatively warm, and fresh CC surface water ~200 km offshore (Figure 3).

### 3.2. Biogeochemical Conditions

#### 3.2.1. Macronutrients and Dissolved Iron

Nitrate ($NO_3^-$) and silicic acid ($Si(OH)_4$) were elevated in recently upwelled Chla-rich water masses (Figure 4). The MBF had an initial surface concentration of ~10 µM $NO_3^-$ and ~9 µM $Si(OH)_4$. Similarly elevated concentrations

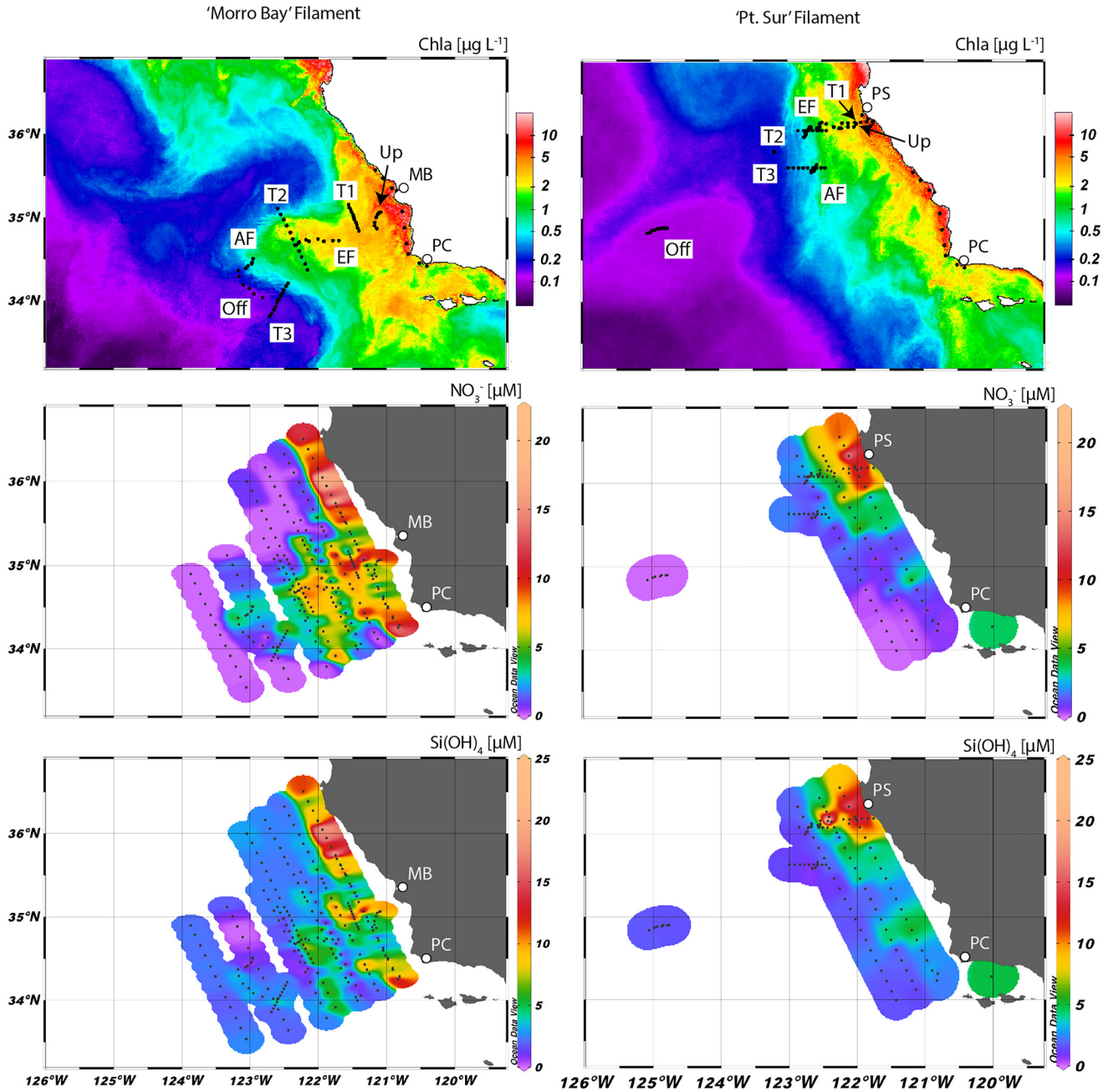


**Figure 4.** Surface plots of Chla (top), nitrate (middle row), and silicic acid concentrations (bottom). Important locations on the California coast are indicated in the maps: Morro Bay (MB), Pt. Conception (PC), and Pt. Sur (PS). Cycle and transect stations are labeled in the top panels. Chla satellite maps are composite images for the time periods 9 June 2017 to 25 June 2017 ("Morro Bay" filament) and 5 August 2019 to 3 September 2019 ("Pt. Sur" filament). Chla data courtesy of Mati Kahru (Scripps Institution of Oceanography).

of macronutrients were found in the PSF shoreward endmember, with initial surface concentrations of ~10 µM $NO_3^-$ and ~13 µM $Si(OH)_4$. Given similar initial concentrations, the PSF showed greater decrease of the macronutrient concentrations relative to the MBF during lateral advection. By the end of the filament studies, surface waters were heavily depleted of $Si(OH)_4$ (<1 µM) but contained some remaining $NO_3^-$ (3.5 and 1 µM for the MB and PSFs, respectively).

The MBF BBL endmember had an elevated concentration of 14.77 nmol $L^{-1}$ dFe. Nearshore surface waters, where Cycle MBF-Up was initialized, had a concentration of ~1.2 nmol $L^{-1}$ dFe. Over all cycles, concentrations

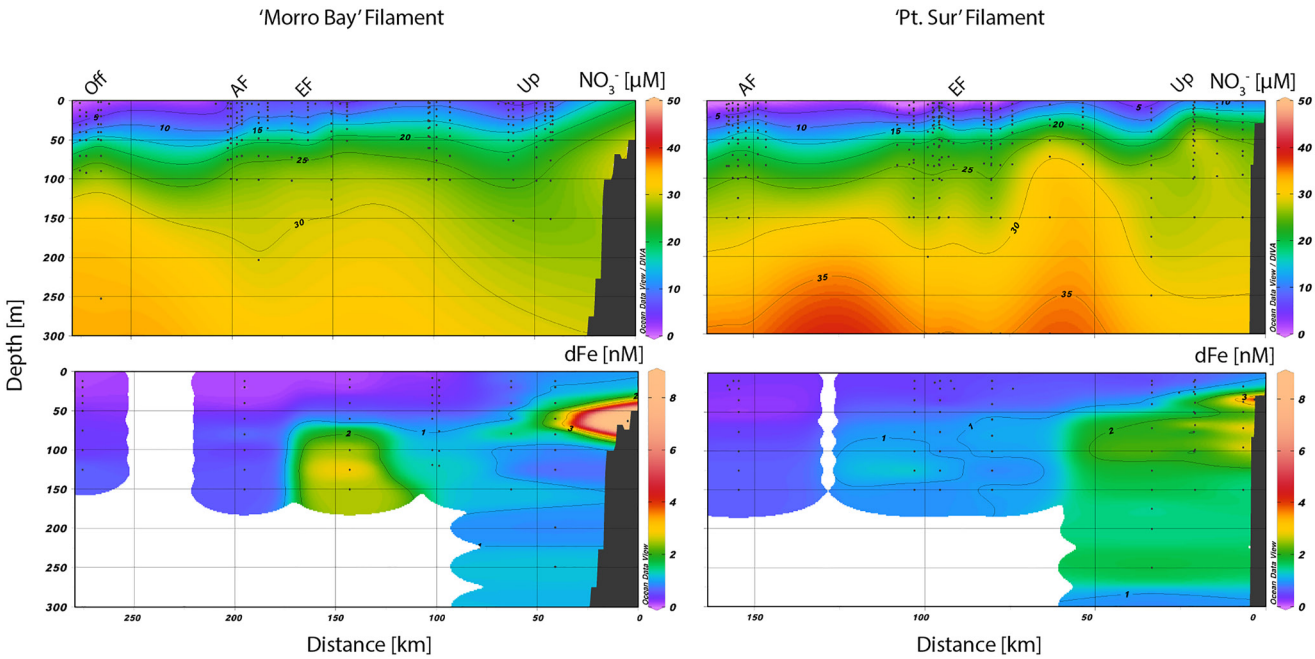


**Figure 5.** Concentrations of $NO_3^-$ (top) and dFe (bottom). These variables are plotted as sections, generally as a function of distance transported (according to Figure 2) within the "Morro Bay" (left) and "Pt. Sur" (right) filaments.

of dFe decreased in the surface (Figure 5), and quickly reached levels less than 0.2 nmol $L^{-1}$ dFe in Cycle MBF-EF, where concentrations remained low in the offshore cycles. An elevated dFe plume was observed ~50 km offshore at depths of 50–75 m. A subsurface dFe maximum of 2–3 nmol $L^{-1}$ occurred between 75 and 150 m depth, approximately 140 km along the filament track at Cycle MBF-EF Day 4 profile.

The PSF BBL endmember had a concentration of 8.49 nmol $L^{-1}$. This dFe rich plume extended only 35 km along the filament track, at a depth of ~40 m. Profiles from Cycle PSF-Up showed a thick (50–250 m depth) ~3 nM dFe signature close to the continental slope (Figure 5). Like the MBF, dFe concentrations in the surface decreased along the filament track although concentrations approaching 0.2 nmol $L^{-1}$ were not observed until Cycle PSF-AF. Cycle PSF-EF had surface (<25 m) concentrations around 0.4–0.6 nmol $L^{-1}$ dFe. A deep maximum in dFe (1.5 nmol $L^{-1}$) was found ~100 km along the PSF track at the Cycle PSF-EF Day 4 profile, similarly identified during the MBF.

### 3.2.2. Labile Particulate Iron, Biogenic Silica, and Particulate Organic Matter

Cycle PSF-Up profiles of labile particulate Fe (LpFe = TDFe − dFe) are shown in Figure S1 in Supporting Information S1. The PSF had subsurface maxima in LpFe for the first 2 days of the cycle (days 1 and 2). The PSF-Up day 4 profile, which is furthest from the continental margin, had similar concentrations to the MBF-Up day 1 profile. At this station, a maximum of ~8 nmol $L^{-1}$ LpFe was observed in the surface and this decreased with depth. Water column bSi and POC measurements were highest in Cycles Up and EF for both cruises (Figure 6). While bSi and POC maxima were restricted to the euphotic zone (<50 m), LpFe and beam attenuation coefficient (beam c) showed surface and subsurface maxima. Beam c had highest absolute values in the euphotic zone, where biogenic particles associated with the phytoplankton bloom were present. Close to the continental margin, elevated beam c and LpFe co-occur indicating potential resuspension of shelf sediments. This was most clearly observed for the MBF. A prominent turbid plume was not detected during the PSF, however, elevated LpFe concentrations coincided with higher dFe in profiles adjacent to the margin sediments.

The trends in bSi and POC for the MBF showed that bSi and POC generally increased through Cycle MBF-Up, and then decreased after reaching maximum values in Cycle MBF-EF (bSi 3.15 µmol $L^{-1}$, POC 41.12 µmol $L^{-1}$; Figure 6) indicating the dynamic nature of biogenic particles during a bloom cycle in upwelled waters. These changes were accompanied by a deepening of the Chla maximum as the filament moved offshore. MBF-Off had significant reductions in bSi (average 0.61 µmol $L^{-1}$) and POC (average 7.39 µmol $L^{-1}$) concentrations

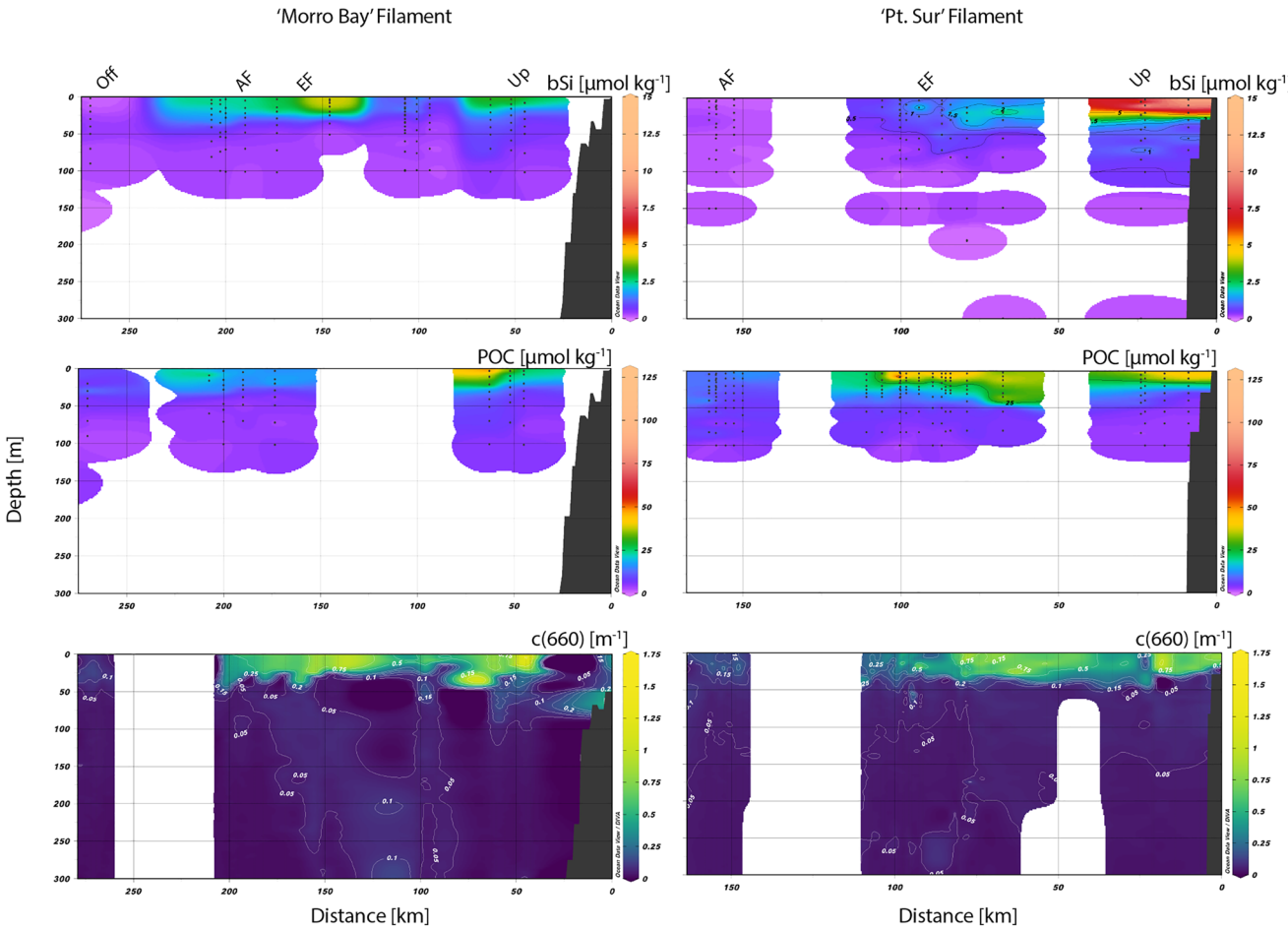


**Figure 6.** Concentrations of bSi (top) and particulate organic carbon (middle) are plotted with beam attenuation coefficient at 660 nm (bottom). These variables are plotted as sections, generally as a function of distance transported (according to Figure 2) within the "Morro Bay" (left) and "Pt. Sur" (right) filaments.

within the euphotic zone. During the PSF cruise, concentrations of bSi were greatly elevated in surface waters in Cycle PSF-Up (range 3.1–11.4 µmol $L^{-1}$), but quickly decreased by Cycle PSF-EF (0.38–1.36 µmol $L^{-1}$). Within surface waters during Cycle PSF-AF, bSi was similar to offshore concentrations (<0.1 µmol $L^{-1}$). Nearshore POC concentrations increased during Cycle PSF-Up (from average of 16.9 to 27.5 µmol $L^{-1}$), followed by an increase to the highest measured concentrations in Cycle PSF-EF (average 34.9 µmol $L^{-1}$). Finally, Cycle PSF-AF had low concentrations of POC at the surface (average 10.2 µmol $L^{-1}$).

### 3.2.3. Benthic Boundary Layer Transects

We conducted repeat surveys of BBLs at 9 stations located on the continental shelf extending from Cambria to just south of Pt. Conception (PC) (Figure 7) to measure dFe, TDFe, dissolved manganese (dMn), and total dissolvable Mn (TDMn). In summer 2017, the concentrations of dFe ranged from 2.4 (station 1) to 15 nmol $L^{-1}$ (station 4) with an average of 8.77 ± 4.41 nmol $L^{-1}$. TDFe concentrations ranged from 140 (station 1) to 719 nmol $L^{-1}$ (station 4) with an average of 424 ± 227 nmol $L^{-1}$. We observed a similar pattern with dMn, where station 4 had elevated levels compared to adjacent stations, however, the highest concentrations of dMn were observed at stations 7 and 9 (5.41 and 5.81 nmol $L^{-1}$, respectively). The highest concentration of TDMn was found at station 7 (13.0 nmol $L^{-1}$), followed by stations 3 (12.2 nmol $L^{-1}$) and 4 (11.6 nmol $L^{-1}$). Like the summer 2017 transect, concentrations of dFe and TDFe during 2019 were highest at station 4 (27.0 nmol $L^{-1}$ dFe, 1,175 nmol $L^{-1}$ TDFe). Compared to the 2017 transect, the average concentrations of dFe (11.4 ± 8.10 nmol $L^{-1}$) and TDFe (546 ± 284 nmol $L^{-1}$) were higher and with greater variability in dFe among stations. At the shoreward PSF region of upwelling, three BBL stations were sampled (Figure 7a). Station 2 was considered as the PSF shoreward endmember, located within the zone of upwelling. The PSF region BBL stations had an order of magnitude

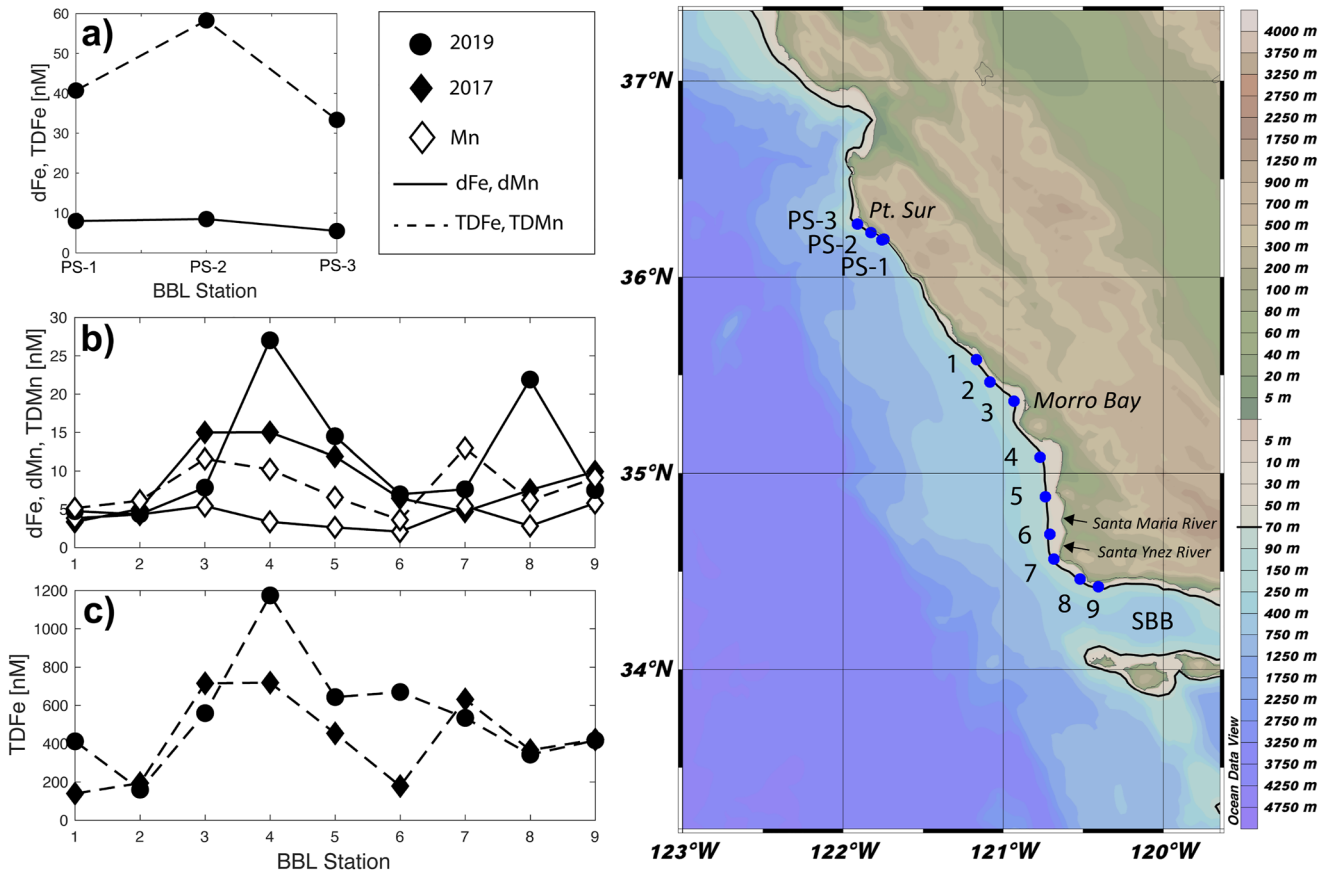


**Figure 7.** The map shows stations for the benthic boundary layer (BBL) Transect, a series of stations sampled along the Californian coast. The black contour denotes the approximate 70 m isobath. SBB is the Santa Barbara Basin. (a) Dissolved Fe (black solid line) and total dissolvable iron (TDFe, black dashed line) trace metal concentrations found within the BBL in Pt. Sur stations in summer 2019. (b) Dissolved Fe (2017 solid line with black diamonds, 2019 solid line with circles), dissolved Mn (dMn, 2017 solid line with white diamonds), total dissolvable manganese (TDMn, 2017 dashed line with white diamonds) trace metal concentrations found within the BBL transect. (c) Total dissolvable iron (TDFe, 2017 dashed line with black diamonds, 2019 dashed line with circles) trace metal concentrations found within the BBL stations in summer surveys. Stations are labeled by numbers 1—*Cambria*, 2—*Pt. Estero*, 3—*Morro Bay*, 4—*Line 77.49*, 5—*Vandenberg*, 6—*Santa Ynez*, 7—*Pt. Aguello*, 8—*Line 80.51*, 9—*Gato*.

lower TDFe concentrations (33.4–58.3 nmol $L^{-1}$) than in the 2017 and 2019 BBL transects, but similar dFe concentrations.

### 3.3. Incubations

Bioassay experiments provide direct evidence of Fe stress. Significant increases in biomass (i.e., Chla) and macronutrient uptake were observed in incubation bottles amended with +Fe and +Fe/+N. For the MBF, greater uptake of $NO_3^-$ and increases in Chla were observed in the +Fe treatment compared to the unamended control bottles (i.e., Fe-limitation) in four of five incubations (Figure 8). Cycle MBF-Up Day 1 was the only location which did not show a significant response to +Fe treatment, and therefore was considered Fe replete. Rapid increases in Chla biomass and net $NO_3^-$ uptake occurred during Cycle MBF-EF incubations, with ~8 µmol $L^{-1}$ $NO_3^-$ drawdown by the +Fe treatment within 24 hr of Cycle MBF-EF Day 1 incubation. A similar response occurred in Cycle MBF-EF Day 4 and Cycle MBF-Off Day 1 incubations, although $NO_3^-$ concentrations remained nonzero up to 48 hr following +Fe. Following exhaustion of $NO_3^-$, Chla declined. The Cycle MBF-AF Day 2 incubation only showed evidence of Fe stress after 3 days. Surprisingly, no significant differences in the uptake of $Si(OH)_4$ was observed in any of the treatments and incubations.

Fe-limitation of the phytoplankton community was tested during the PSF and was observed in three of the four +Fe amendment studies. Like the MBF, Fe replete conditions were found to occur at Cycle PSF-Up Day 2, close to shore (Figure 9). Cycle PSF-EF Day 2 and Cycle PSF-EF Day 3 incubations were characterized by

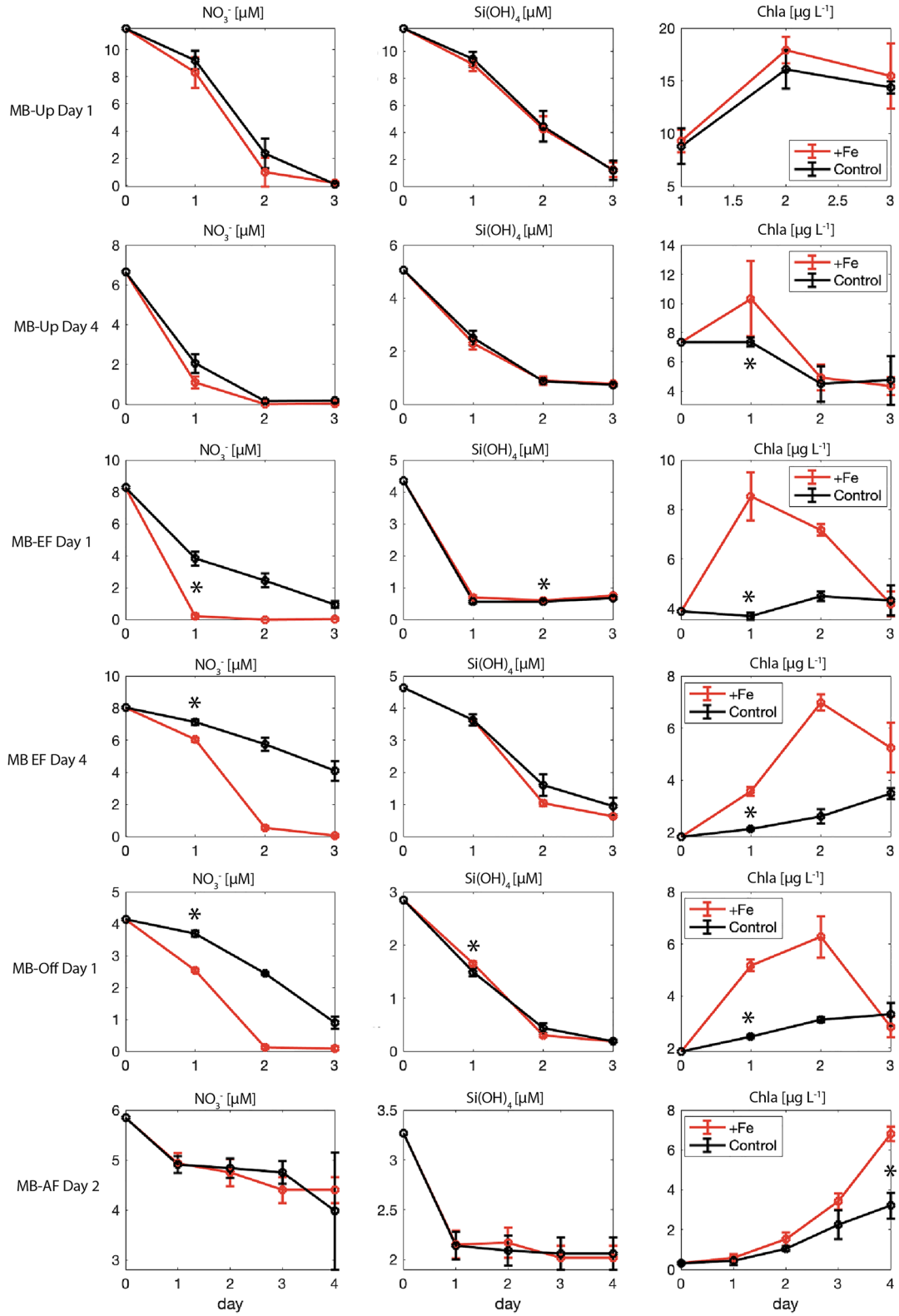


**Figure 8.** Growth and nutrient uptake monitored during deckboard incubation experiments during the "Morro Bay" filament cruise (P1706). The cycle and day for experiment initiation (day = 0) is indicated for each row. The left column is $NO_3^-$ concentration, middle column is $Si(OH)_4$ concentration, and the right column is Chla concentration as a proxy for biomass. These experiments correspond to the number labels in Figure 2. The * denotes the first timepoint in which a significant difference in the +Fe treatment and unamended control Chla concentration means are observed (paired *t*-test, $p < 0.05$).

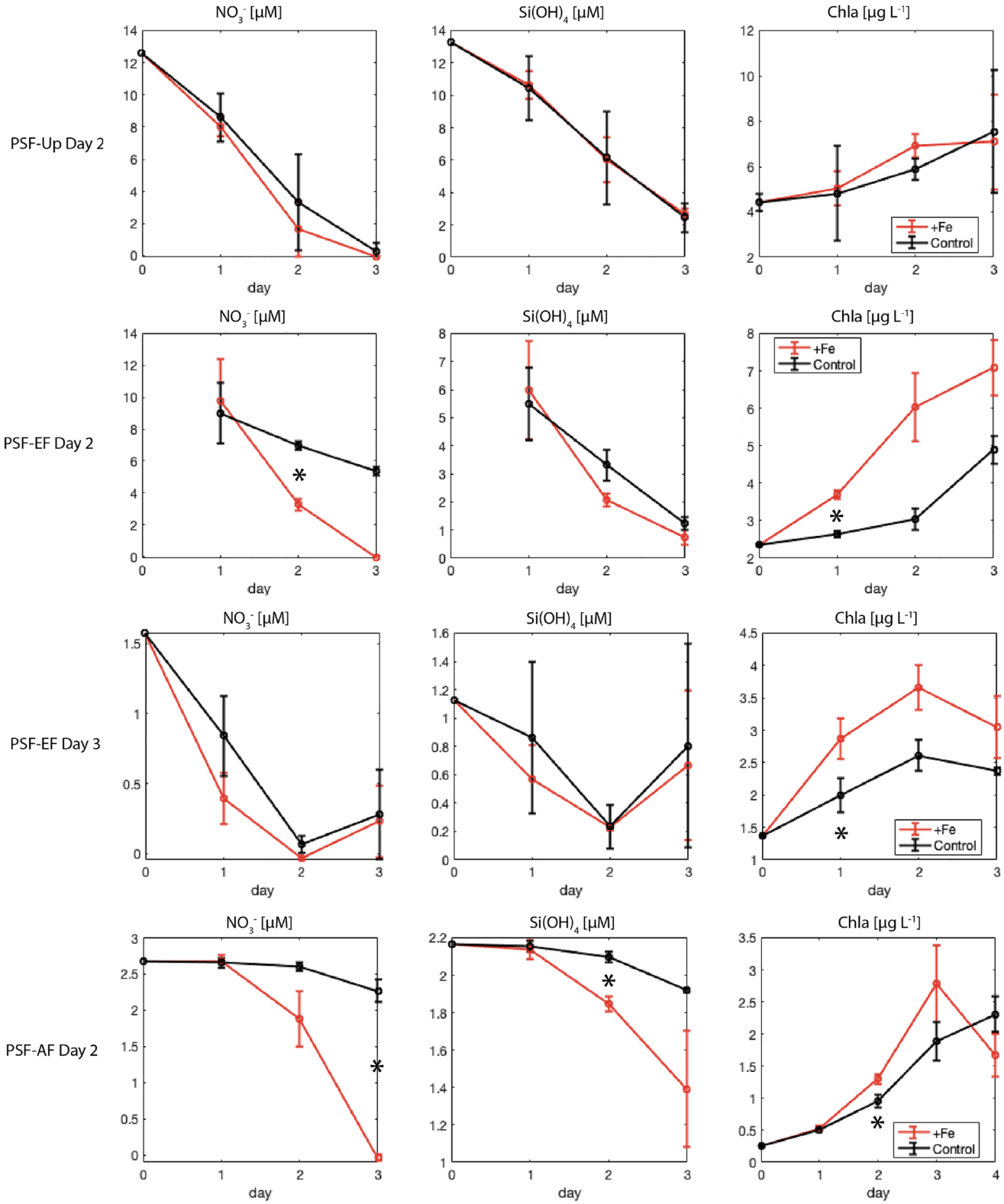


**Figure 9.** Growth and nutrient uptake monitored during deckboard incubation experiments during the "Pt. Sur" filament (PSF) cruise (P1908). The cycle and day for experiment initiation (day = 0) is indicated for each row. The left column is $NO_3^-$ concentration, middle column is $Si(OH)_4$ concentration, and the right column is Chla concentration as a proxy for biomass. Experiment names correspond to the number labels in Figure 2 (except for PSF Cycle Off experiment which is labeled as 5). The * denotes the first timepoint in which a significant difference in the +Fe treatment and unamended control Chla concentration means are observed (paired *t*-test, $p < 0.05$).

Fe-limitation, where +Fe treatments consumed $NO_3^-$ and accumulated Chla faster than the control. However, the results are less obvious for Cycle PSF-EF Day 3, which was initialized with surface water containing lower $NO_3^-$ (1.5 nmnol $L^{-1}$). Cycle PSF-AF Day 2 +Fe treatment showed a strong response but was not significantly different from the control until 24 hr. Unlike all other incubations where Fe limitation was observed, a significant increase in the uptake rate of $Si(OH)_4$ was found in the +Fe treatments of Cycle PSF-EF Day 2 and Cycle PSF-AF Day 2 incubations.

Co-limitation of Fe and $NO_3^-$ was observed in the far offshore Cycle PSF-Off incubation (Figure S2 in Supporting Information S1). Following 48 hr of incubation, no growth was observed in the control, but greater Chla concentrations were observed in the +Fe, +N, and +Fe/N treatments, in order of increasing growth response. To determine if there were significant differences among the treatments, an analysis of variance (ANOVA) test was performed. The results of the ANOVA test indicate a significant effect of treatment on Chla concentration ($F$-value = 4.82, $p < 0.05$). To further investigate pairwise differences between the means, Tukey's Honest Significant Difference post hoc test was conducted. Significant differences were found between the control and +N group ($p = 0.021$), control and +Fe/N group ($p = 0.009$), +N and +Fe ($p = 0.034$), and +N and +Fe/N group ($p = 0.017$). These results indicate the addition of dFe and $NO_3^-$ individually, as well as their combined addition, have distinct effects compared to the control.

In all instances where the addition of Fe stimulated additional Chla production, there was a corresponding increase in the POC concentration, but no difference between treatments in the bSi concentration (Incubations 2–5 MBF, 2–4 PSF). Additional POC within the +Fe treatments in these incubations resulted in a significantly lower bSi:POC ratio (Figure 10), however the difference in bSi:POC ratio between the +Fe and control in the PSF were smaller than in the MBF.

### 3.4. Export

Export flux of sinking particulate matter was investigated in both filaments and presented as per day averages over the duration of the cycle, as shown in Figure 11. For the MBF, bSi export was highest at the base of the euphotic zone and in Cycle MPF-Up (16 mmol Si $m^{-2}$ $day^{-1}$), followed by Cycle MBF-AF (11 mmol Si $m^{-2}$ $day^{-1}$), while the lowest export was found at Cycle MB-Off outside of the filament (3.5 mmol Si $m^{-2}$ $day^{-1}$). POC export for the MBF was highest at the base of the euphotic zone in Cycles EF (44 mmol C $m^{-2}$ $day^{-1}$), Cycle Off (47 mmol C $m^{-2}$ $day^{-1}$), and Cycle EF.5 (46 mmol C $m^{-2}$ $day^{-1}$), however flux magnitude decayed exponentially with increasing depth. The POC flux in the deepest trap in Cycle MBF-AF (26 mmol C $m^{-2}$ $day^{-1}$ at 169 m) attenuated 28% from the flux at base of the euphotic zone (36 mmol C $m^{-2}$ $day^{-1}$ at 56 m). Higher POC export was measured in the PSF compared to the MBF. The highest POC export was found to occur at Cycle PSF-AF at the base of the euphotic zone (53 mmol C $m^{-2}$ $day^{-1}$). The PSF followed a similar trend toward higher POC export values during offshore cycles. However, compared to the MBF, lower bSi export occurred during all cycles (0.26–7.1 mmol Si $m^{-2}$ $day^{-1}$). Generally, the bSi and POC export magnitude tracked each other during both cruises, except for MBF-Up, which had the highest bSi export flux among cycles, but the second lowest export of POC.

## 4. Discussion

### 4.1. Fe Limiting Conditions and Macronutrient Ratios in Upwelling Filaments

From the standpoint of Fe biogeochemistry in the CCE, the PSF sampling stations are of particular interest, because the Big Sur upwelling region has been characterized as chronically Fe limited. Hutchins et al. (1998) contrasted the Big Sur upwelling and filament region with the Mendocino shelf region further north, to make the case that spatial variation in the mud-belt shelf width and riverine input along the CCE region is a key factor in determining the Fe-limitation status of upwelling waters (Hutchins et al., 1998). With narrow shelf widths and low riverine input, the MB and PSF regions are likely candidates for potential Fe-limitation, especially given that Fe-limitation has been shown even with moderate shelf widths in upwelling areas (Till et al., 2019). Whether the parcel of water is beyond the shelf break is an additional indicator for upwelled waters to become Fe limited. These results highlight the need to further examine the link between sampling location and time with respect to Fe-limitation.

Biomass limitation by Fe (Liebig limitation) can be approximated using the $NO_3^-$:dFe ratio because coastal diatoms have an optimal uptake ratio required for their cellular components. Ratios exceeding 10–12 μM:nM are indicative of a nutrient regime that is likely to become Fe-limited because diatoms lack sufficient Fe to

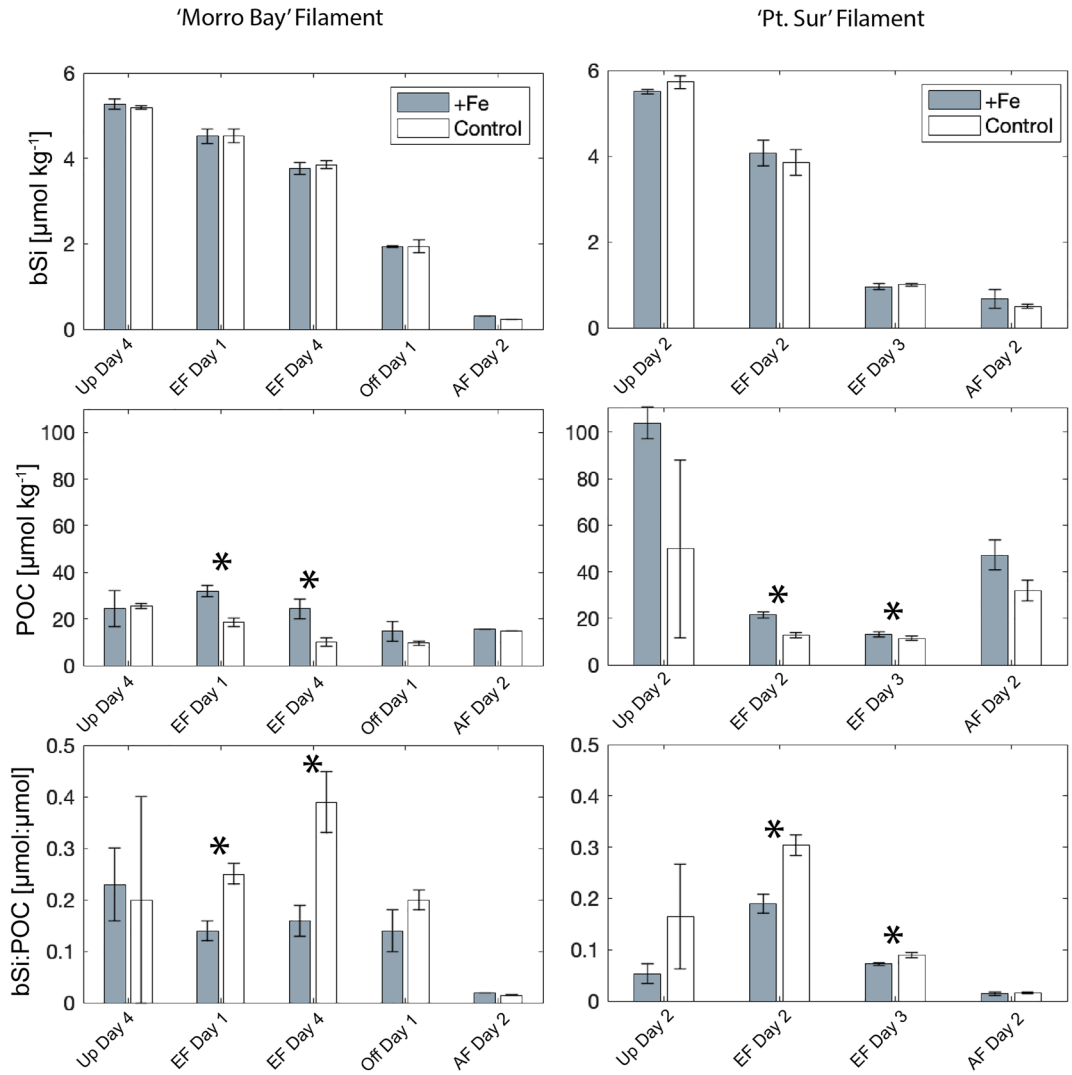


**Figure 10.** Final timepoint measurements of bSi (top), particulate organic carbon (POC) (middle row), and bSi:POC ratios (bottom) for deckboard incubations according to Cycle labels in Figure 2. The * denotes a significant difference in the +Fe treatment and unamended control (paired *t*-test, $p < 0.05$).

consume the surface $NO_3^-$ completely (King & Barbeau, 2007). Additionally, Fe limited diatoms may preferentially deplete the water of $Si(OH)_4$ over $NO_3^-$ (Brzezinski et al., 2015; Firme et al., 2003; Franck et al., 2000, 2003; Hogle et al., 2018; Hutchins & Bruland, 1998; Krause et al., 2015; Takeda, 1998), decreasing in situ $Si_{ex}$ and leaving a compounding signature of Fe-limitation. By utilizing both the in situ $NO_3^-$:dFe ratio as well as $Si_{ex}$, we can gain insight into where coastal upwelling filaments exhibit evidence for Fe-limitation.

Diatoms dominated the MBF phytoplankton community, contributing most to biomass and Chla (Figure S3 in Supporting Information S1). Mixed layer $Si_{ex}$ values decreased significantly in Cycle MBF-EF, compared to Cycle MBF-Up, and remained low in Cycle MBF-AF (Figure 12). These changing uptake rates of macronutrients suggest that dFe was rapidly consumed between Cycles Up and EF, resulting in an Fe-limited diatom community, which preferentially depleted the surface of $Si(OH)_4$ relative to $NO_3^-$ (low $Si_{ex}$). This was also reflected in the $NO_3^-$:dFe, which exceeded >100 µM:nM, indicating the potential for strong Fe limitation. These high values have only been observed in chronically Fe-limited regions of the ocean, such as the Gulf of Alaska and the Southern Ocean (Hopwood et al., 2020). The onset of significant Fe-limitation of the bloom was captured in the Cycle MBF-EF Day 1 incubation (Figure 8), where complete exhaustion of the $NO_3^-$ pool occurred within 24 hr of Fe addition. Rapid accumulation of Chla and consumption of $NO_3^-$ was also observed for the Fe addition treatments in Cycle MBF-EF Day 4 and Cycle MBF-Off Day 1 incubation experiments. These were conducted

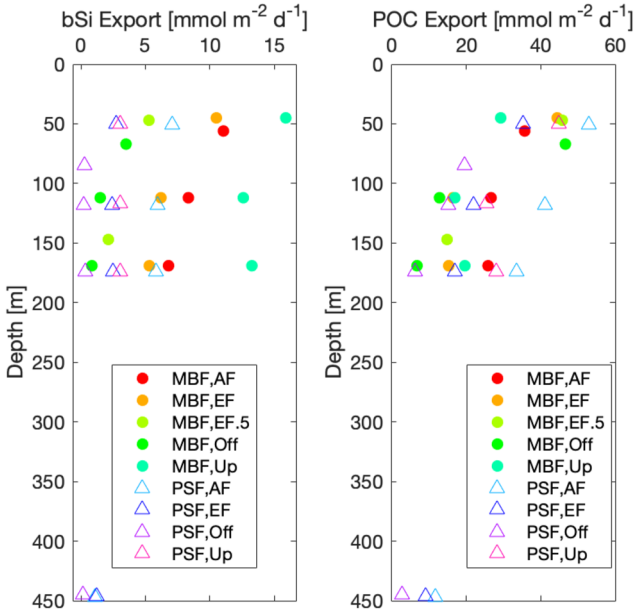


**Figure 11.** Measured sediment trap export flux of biogenic silica (bSi) and particulate organic carbon (POC) for the "Morro Bay" (circle symbols) and "Pt. Sur" Filaments (triangle symbols). Units for bSi and POC export flux are in mmol $m^{-2}$ $day^{-1}$. Colors of symbols correspond to the "Cruise" and "Cycle" numbers indicated by the legend. Cycle early filament (EF).5 corresponded to a sediment trap which remained in the Cycle EF Day 4 water mass.

using surface water from off the shelf break (Figure 2). In the Cycle MBF-AF Day 2 incubation, phytoplankton growth was slower, and Fe-limitation was not observed to be significant until the third day post Fe addition (Figure 8), likely due to the degree of senescence occurring within the bloom. In all incubations that indicated some degree of Fe-limitation, the control Si:N uptake ratios were greater than 1:1 and higher than the +Fe treatments, after just 24 hr. These results support the hypothesis of Chavez et al. (1991), that regional waters advected offshore with their phytoplankton populations will become Fe limited.

Due to the high concentrations of bSi within the PSF, it is assumed that in Cycle PSF-Up and for the first few days of Cycle PSF-EF, the phytoplankton community was dominated by diatoms (Figure S3 in Supporting Information S1). However, surface $NO_3^-$:dFe ratios decreased in Cycle EF and AF (Figure 12), driven by decreasing concentrations of $NO_3^-$ (Figure 5). This suggests a community with weak Fe limitation, which is confirmed by incubations from these cycles showing some evidence of Fe-limitation of the phytoplankton community but to a lesser degree than observed in MBF (Figure 9). In all incubations that indicated some degree of Fe-limitation, the control Si:N uptake ratio was greater than 1:1 and higher than the +Fe treatments, although it took 2–3 days to resolve these net effects. In PSF-AF, low Si:N uptake ratios (~0.8) were observed throughout the experiment, with only a slight decrease in the +Fe treatment, relative to the control. This indicates that the whole community was stimulated by Fe and that diatoms may have been Si-limited.

Metagenomic assessments of the eukaryotic communities showed that phytoplankton communities of inshore Cycles (Up and EF) from the PSF were dominated by high relative abundance of pennate (*Pseudo-nitzschia*) and large chain-forming and centric diatom (*Chaetoceros*, *Thalassiosira*) sequences. A shift to smaller phytoplankton (e.g., the picoeukaryote *Pelagomonas*) occurred in offshore cycles as the Chla maximum deepened (Figure S3 in Supporting Information S1, Lampe et al., under review). Compared to the PSF, the MBF contained much greater relative proportions of *Pseudo-nitzschia* (Sara Rivera, personal communication), a pennate diatom, which are able to acquire additional dFe as luxury Fe and store it intracellularly as ferritin (Marchetti et al., 2006). Further, pennate diatoms are able to maintain relative Fe quotas 10 times higher than centric diatoms due to this enhanced ability for storage (Twining et al., 2021). Together with intense scavenging onto particles, phytoplankton community composition could explain the rapid depletion observed in surface dFe concentrations between Cycles Up and EF in the MBF, although a quantitative assessment of pennate versus centric diatom contributions to the phytoplankton community Fe demand is outside the scope of this paper. The MB and PSFs had different relative proportions of pennate and centric diatoms in Cycles Up and EF, which may suggest that different $NO_3^-$:dFe ratios might be more appropriate threshold indicators for potential Fe-limitation given the different diatom assemblages. In both filaments, the formation of subsurface chlorophyll maxima at Cycles AF and Off led to shifts from diatom communities toward picoeukaryotes known to inhabit deep nitraclines in the CCE (Hogle et al., 2018). These subsurface chlorophyll maxima communities located at the top of the nitracline exhibit Fe and $NO_3^-$ co-limitation (Figure S2 in Supporting Information S1) and could be a widespread biochemical condition for eukaryotic and prokaryotic primary producers over vast regions of the oligotrophic ocean where subsurface chlorophyll maxima are ubiquitous, but where light is likely a strong factor.

The geochemical indicators of Fe stress ($NO_3^-$:dFe, $Si_{ex}$) correspond with direct evidence of Fe stress from incubation studies which point toward diatom growth being Fe limited off the shelf break, consistent with the hypothesis of the upwelling filament transitioning from nutrient replete to Fe limiting for diatom growth as it moves offshore (Figure 1). In aging water masses, phytoplankton are thought to satisfy their Fe demand from remineralized sources of dFe (Rafter et al., 2017) or from labile Fe particles via organic ligand solubilization (Milne et al., 2017) on timescales of particle sinking in the euphotic zone. Based on our observations, diatoms are not meeting their Fe demand in aging filaments, but other phytoplankton are since a shift in the community composition was

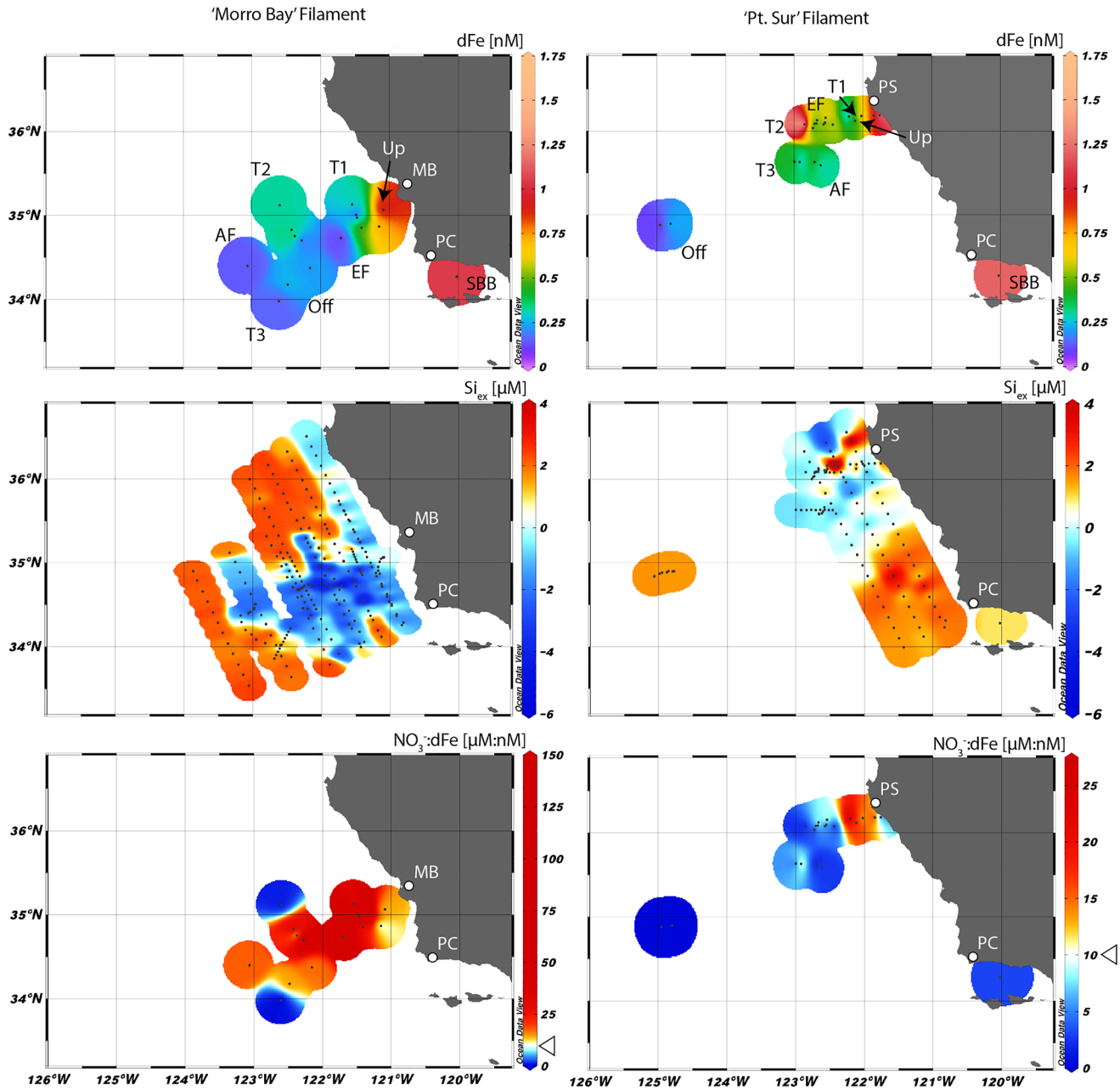


**Figure 12.** Surface plots of dFe (top), $Si_{ex}$ (middle row), and $NO_3^-$:dFe ratio (bottom). Important locations on the California coast are indicated: Morro Bay (MB), Pt. Conception (PC), and Pt. Sur (PS). Cycle and transect stations are labeled in the top panels. Color scale $NO_3^-$:dFe ratio is set to white at 10 µM:nM, which is an indicator threshold of possible Fe limitation of diatom communities in incubation experiments (King & Barbeau, 2007).

observed. Filaments are more horizontally advective environments and the ferricline and nitracline decouple as filaments age (Figure 5) because remineralization rates of particulate Fe are slower than for particulate nitrogen.

### 4.2. Sources of Fe to Upwelling Filaments

#### 4.2.1. Sediments Within the BBL

The continental shelf is a well-studied dFe and TDFe-rich source (Elrod et al., 2004) and relationships between the shelf width, winter storms, riverine deposition of lithogenics and Fe concentrations within the BBL are established (Chase et al., 2005, 2007). These historical insights of Fe content of upwelled waters are considered

first-order controls, describing Fe concentrations in a predictable spatial context. The assemblage of Fe-binding organic ligands was shown to be distinct within the BBL compared to surface and offshore waters (Bundy et al., 2014), adding nuance to our simplified perspective of Fe supply from margin sediments. Adding to this complexity, we speculate on the effect of additional controls, including particle concentration and DO, by leveraging the BBL data set from the MBF cruise in summer 2017.

The dFe and TDFe content of MBF cruise BBL stations 3, 4, 7, and 9 were elevated relative to other stations (Figure 9). Since TDFe and TDMn may be related to the suspended particulate mass, from profiles of beam transmission we found that stations 3, 4, and to a lesser extent station 7, had thick bottom suspensions of particles at the time of sampling (Figure S4 in Supporting Information S1). Beam attenuation coefficient is correlated with TDFe ($r^2 = 0.78$, $p < 0.00001$, $n = 21$) when considering all BBL data collected in summers 2017 and 2019, indicating the expected first-order control of sediment resuspension on Fe concentrations. The relationship between dFe and suspensions of particles ($r^2 = 0.59$, $p = 0.0048$, $n = 21$) is, however, less straightforward, since adsorption sites compete with organic Fe-binding ligands to scavenge dFe (Ardiningsih et al., 2020). Such high concentrations of dFe in BBL waters could be explained by the excess of organic material available in sediments to bind and stabilize dFe from returning to particulate form (Bundy et al., 2014). Therefore, the nature of this dFe is most likely a mixture of Fe mineral colloids and soluble organic Fe-ligand complexes.

DO in the CUC is declining (Ren et al., 2018), and the areal extent of sediments in contact with low oxygen water masses may increase (Dussin et al., 2019). Bottom water DO may be an additional control, adjusting the relative proportions of soluble Fe flux from sediments (as reduced Fe(II)) and co-occurring Fe-oxy(hyr)oxide colloids (Burdige & Komada, 2020; Dale et al., 2015). Fluxes of reduced Fe from sediments rapidly oxidize at the sediment-seawater interface. To investigate this point further, we plotted DO profiles for the nine stations from the 2017 BBL survey (Figure S4 in Supporting Information S1). Manganese (Mn), similar to Fe, undergoes dissimilatory reductive cycling in marine sediments, however, its abiotic oxidative half-life is $\sim 10^6$ times that of Fe(II) and is therefore a good tracer for recent sedimentary input (Sherrell et al., 2018). A comparison of dFe and dMn concentrations at the summer 2017 BBL stations 3 and 4 with station 7 is suggestive of the potential importance of bottom water DO on the sensitive redox behavior of dFe. Stations 3 and 4 have bottom water DO of ~72 μmol $kg^{-1}$, relatively high dMn concentrations, and the highest dFe concentrations measured (~15 nM). At station 7, bottom water DO is ~112 μmol $kg^{-1}$, dMn concentration is similar to BBL stations 3 and 4, yet dFe concentrations are greatly reduced (4 nM). This indicates bottom water DO could regulate the dFe-to-dMn supply ratio from the BBL, since dFe is rapidly oxidized and converted to insoluble particles once in the water column, if equilibration with strong Fe-binding ligands is absent.

The summer 2019 BBL transect overall had a greater range in dFe and TDFe concentrations compared to the 2017 transect, despite having overall higher DO concentrations (126–183 μmol $kg^{-1}$). This suggests that the conditions were not similar between the two cruises at the time of sampling. We do not have corresponding measurements of Mn for the 2019 survey, but future work might utilize differences in redox kinetics of Fe and Mn through trace metal ratios. Among all stations sampled on both cruises, we do not find an overall relationship between dFe concentrations and bottom water DO ($r^2 = 0.03$, $n = 21$). Within the BBL, the depth sampled was found to strongly correlate with dFe and TDFe, which we interpret as the ability to sample close to the sediments depending on shipboard personnel, sampling configuration, and ocean sea state. In summer 2019, our samples were taken closer to the sediments and had correspondingly higher dFe concentrations. The PSF BBL stations had an order of magnitude lower TDFe concentrations compared to the transect further south. This is consistent with observations of Fe-limitation in this region, which were attributed to a zone of poor sedimentary Fe accumulation because of the narrow shelf and lack of fluvial inputs (Hutchins et al., 1998). The Santa Maria and Santa Ynez rivers discharge closest to BBL stations 4–7, but these stations do not consistently contain the highest concentrations of dFe, suggesting considerable deviation from trends found in the northern CCE (Chase et al., 2005). Therefore, local factors must be considered. Inner shelf dynamics are important for the formation of BBLs, but the longevity of these turbid layers has not been investigated despite the important implications for dFe scavenging and timing with upwelling and coastal filament formation. More statistical approaches and continued monitoring of these stations are required to understand the relative strengths of upwelling currents, winter riverine discharge, local circulation, topography, Fe-binding organic ligands, and DO on setting the Fe content of these waters.

#### 4.2.2. California Undercurrent

In the MBF cruise, the CUC was the primary water mass composing the cross-shore advected waters (Zaba et al., 2021). Low-oxygen CUC water can impinge on the shelf during times of upwelling. In the current paradigm

(Figure 1), the degree to which the CUC contributes to the upwelled Fe source has been overlooked as a significant source of Fe in the CCE. The PSF showed much higher subsurface concentrations of dFe and TDFe (2–3 nM and 30–60 nmol $L^{-1}$, respectively) adjacent to the shelf slope, compared to the MBF (0.5–1 nmol $L^{-1}$ dFe) (Figure 5 and Figure S1 in Supporting Information S1). In the MBF, a dFe maximum was found ∼100 km offshore at 75–150 m depth, which could be an offshore signature of the CUC, although it is expected to be found closer to the coast during the summer months (Kurczyn et al., 2019; Rudnick et al., 2017).

Summertime climatological maps of the CCE indicate that the CUC is located close to the shelf slope (centered 50 km offshore) off PC (Rudnick et al., 2017). Further north, near Monterey Bay, the CUC core is found 75–100 km offshore, but can be found in the subsurface up to 150 km from the coast. The elevated concentrations of dFe (∼2–3 nmol $L^{-1}$) in the MBF subsurface offshore waters match those found in the inshore profiles during the PSF, with similarly elevated salinity (33.75–34 PSU) but lower DO (50–100 μmol $kg^{-1}$, Figure S5 in Supporting Information S1). Generalizing water mass climatologies for the MB and PSF regions and the biogeochemical signatures, the observed dFe subsurface signatures in ocean transects (Figure 5) may be derived from the poleward flowing CUC.

Northward geostrophic currents are intensified near the continental margin during the summer and into the Fall. We hypothesize that the CUC, during its northward transit, may entrain additional dFe and TDFe from resuspended margin sediments and that this is enhanced near prominent headlands during times of wind driven upwelling. Additional local considerations, such as seasonality in internal waves breaking on shelf slopes (Lam et al., 2018) may be important additional mechanisms for suspending Fe-bearing sediments and increasing LpFe in subsurface water masses near the coast. The CUC feeds upwelling water with remineralized sources of macronutrients (Zaba et al., 2021). We suggest such high rates of primary production associated with the CUC may be, in part, explained by its relatively high concentrations of dFe compared to offshore subthermocline water masses which might also be upwelled. The relative contribution of dFe from the CUC and the BBL to upwelled waters should be explored further to accurately predict changes in the primary production potential of upwelled waters in the CCE.

### 4.3. Fe-Limitation and Diatom Community Elemental Stoichiometry

Phytoplankton Fe stress affects light harvesting, carbon acquisition, and $NO_3^-$ assimilation because these are Fe-intensive processes (Hutchins & Bruland, 1998; Morel, 2008). Diatoms, when Fe stressed, remain in cell cycle stages that facilitate slower growth, increasing silicification due to prolonged uptake in such stages (De La Rocha et al., 2000; Smith et al., 2016). When $Si(OH)_4$ is not kinetically or growth limiting, cellular Si (as bSi) content can increase under such conditions, and corresponding reductions in $NO_3^-$ assimilation and carbon fixation lead to net increases in Si:N and Si:C uptake ratios, thereby increasing the bSi:POC ratio (Marchetti & Harrison, 2007). Such cellular reconfigurations can affect the efficiency of carbon export and sequestration, through changing sinking speeds and potentially modifying grazing pressure (Assmy et al., 2013; Brzezinski et al., 2015; Hutchins & Bruland, 1998).

Higher bSi:POC diatom communities are likely to sink faster due to their increased ballast, which could contribute to the observed declines (Brzezinski et al., 2015). Amendment experiment (Figure 10) results support a mechanistic link between the Fe biogeochemical condition and increasing bSi:POC ratios of diatom blooms. Specifically, these results point toward Fe-limitation as a likely driver for elevated bSi:POC ratios, as addition of Fe (alleviation of limitation) increased POC concentrations and lowered bSi:POC ratios. The $Si(OH)_4$ consumption, on the other hand, remained unchanged by the addition of Fe in any of the experiments. While we attributed bSi:POC ratios to physiological changes of diatom communities, a shift in community composition toward more lightly silicified small diatoms would also decrease bSi:POC (Quéguiner, 2013; Tréguer et al., 2018). Other planktonic organisms could affect the observed patterns in bSi:POC, but a quantitative assessment is currently lacking.

Fe-addition grow-out incubations were carried out for ∼3 days, as has been typical in Fe-limitation studies of surface phytoplankton communities. In previous studies in the CC, as well as the Ross Sea, the Humboldt current and the Peru Upwelling (Hutchins & Bruland, 1998; Hutchins et al., 1998, 2002; King & Barbeau, 2007; Sedwick et al., 2000), a 3–4 days incubation timeline, and sometimes up to 7 days (e.g., Burns et al., 2023), captured macronutrient depletion and Chla increases following Fe addition. However, in the MBF incubation studies,

**Table 1**
*Length Scale Parameters for Nitrate, Silicic Acid, and dFe for the "Morro Bay" and "Pt. Sur" Filaments Surface Waters (P1706, P1908, Respectively)*

| Cruise | Nutrient | $r^2$ | $D$ [km] | $n$ |
|---|---|---|---|---|
| P1706 | Nitrate | 0.20 | 399 ± 173 | 103 |
| P1706 | Silicic acid | 0.41 | 155 ± 45 | 103 |
| P1706 | Dissolved Fe | 0.89 | 43 ± 15 | 12 |
| P1908 | Nitrate | 0.44 | 85 ± 18 | 112 |
| P1908 | Silicic acid | 0.45 | 79 ± 18 | 89 |
| P1908 | Dissolved Fe | 0.53 | 250 ± 150 | 22 |

macronutrients in Fe limited Cycles were quickly depleted compared to these previous studies, suggesting a large standing stock of diatoms during our initial conditions (Figure 8). This observed decoupling of nutrient uptake has been observed in and is consistent with previous Fe incubation studies (Hutchins & Bruland, 1998; Till et al., 2019). The Fe acquisition strategies likely differ between the phytoplankton communities, where MBF diatoms might have higher affinity uptake of Fe and are able to divert these few atoms per cell toward assimilating available $NO_3^-$.

### 4.4. Length Scales and Export Efficiency

Macronutrient and dFe concentrations in the filament decrease exponentially with distance from the upwelled water parcel source. Since phytoplankton are present in surface waters, the distribution of dFe in the upper 10–25 m is a function of both uptake by phytoplankton and conversion to other particulate pools because of scavenging. The concentrations ($C$) of dFe, $Si(OH)_4$, and $NO_3^-$ are fit exponentially to the equation:

$$C(x) = C_0 e^{-x/D}$$

where $C_0$ is the concentration of the upwelled water at the surface, $x$ is the distance traveled along the core of the filament during Lagrangian cycles (km), and $D$ is the scale length (km), defined as the distance where $C(x) = 0.37C_0$ (i.e., the concentration has decreased to 37% of the initial concentration, or one $e$-fold). During the MBF, for dFe at 10–25 m, we find [dFe] = $2.673e^{-x/43}$ ($r^2 = 0.89$, $n = 12$, $D = 43 \pm 15$ km, Figure S6 in Supporting Information S1). The PSF had a significantly longer length scale, where [dFe] = $0.687e^{-x/250}$ ($r^2 = 0.53$, $n = 22$, $D = 250 \pm 150$ km, Figure S6 in Supporting Information S1).

The degree of Fe-limitation was found to be more extreme in the MBF, whereas more efficient consumption of the macronutrients occurred during the PSF, suggesting, in part, sufficient concentrations of bioavailable Fe remained within the filament for longer, or the phytoplankton community shifted toward small phytoplankton with lower Fe cellular quotas. Another possibility is that the high concentrations of LpFe within the filament, a mixture of biogenic and authigenic particles, buffered dFe concentrations by keeping them elevated (Milne et al., 2017). These processes are reflected in the length scale parameters for $NO_3^-$ and $Si(OH)_4$ during the PSF, which are 85 ± 18 km and 79 ± 18 km, respectively, compared to 399 ± 173 and 155 ± 45 km in the MBF (Table 1). An important implication of these observations is that Fe-limitation modulates the ability for upwelled nutrients to be advected offshore to the oligotrophic ocean (White et al., 2022).

The efficiency with which bSi and POC are exported from the filament depends on the remineralization efficiency and time spent within the water column, the latter is strongly related to sinking speed. Sinking speed in this sense is related to the density of the particle (Stokesian settling rate), but also the energetics of currents, turbulence, and density gradients. As the filaments accelerate offshore, particles, even large ones, can remain suspended until the current slows and lacks sufficient energy to maintain a particulate suspension. Additional biological processes can greatly affect sinking speeds, such as packaging of cells into fast-sinking aggregates and fecal pellets produced by mesozooplankton grazers (Longhurst & Glen Harrison, 1989).

Stukel and Barbeau (2020) compiled sediment trap export flux data for all CCE Long Term Ecological Research (LTER) process studies, including the MBF (P1706) and found that patterns in the nutrient landscape of the CCE region are better predictors of the flux of sinking particles than measurements of net primary production. Carbon export was found to be enhanced during high-nutrient and Fe-stressed conditions. We investigated the efficiency with which particulate matter is exported from the euphotic zone with relation to the Fe-limitation status of the phytoplankton community. In the MBF, Cycle AF showed the highest export of POC relative to all other cycles, despite having the lowest biomass. The same is true for bSi, except for at Cycle MBF-Up in the ~100 and 150 m traps, which is likely a result of the production of anchovy fecal pellets (Figure 11). Bourne et al. (2021) found these pellets in Cycle MBF-Up were full of diatom frustules and fragments. We found that ~9% of the bSi inventory at Cycle MBF-Up is exported to 150 m, whereas ~24% is exported at Cycle MBF-AF. POC export efficiency shows similar trends with 1.5% and 4.9% of the inventory exported per day for Cycles Up and AF, respectively.

The PSF showed similar export efficiency of POC within the top 50 m in Cycles Up and EF (3.8% per day and 4.0% per day, respectively). However, Cycle PSF-AF reached as high as 11% of the POC inventory exported per day to 50 m. This cycle had the highest values of POC flux measured over both cruises (Figure 11). Far offshore, 3.2% of the POC inventory reached 120 m per day. The bSi export efficiency to 150 m depth was similar between Cycles Up and EF (3.3% per day and 4.2% per day, respectively). An increase to ~27% bSi inventory per day was estimated at Cycle PSF-AF, which is similar to the export in the offshore cycle in the MBF. The oligotrophic Cycle PSF-Off had the lowest export efficiency (2.8% bSi inventory per day). Cycles Up and EF had the highest bSi flux in the PSF, however, these stations also had the highest bSi concentrations measured. It is likely that the high concentrations of bSi accumulated in early stages of the filament remained suspended until Cycle PSF-AF, where incubation results showed the greatest degree of Fe-limitation (Figure 9).

It appears that based on these trends, that within regimes of Fe-limitation, export of biomass is more efficient. These results support the hypothesis put forward by Stukel and Barbeau (2020) and finding of increased diatom-mediated POC export in Fe-limited CCE upwelled waters (Brzezinski et al., 2015). Coastal upwelling filaments are mechanisms by which coastally upwelled waters are advected offshore, resulting in decoupling of net primary production and export (Chabert et al., 2021; Kelly et al., 2018). This decoupling within mesoscale features of the CCE has been described previously and was attributed to lateral transport of high-biomass stages of phytoplankton blooms (Landry et al., 2009; Plattner et al., 2005). We argue that increased ballasting due to Fe-limitation of diatom aggregates and fecal pellets may be an additional control of *where* export occurs. These findings may help better resolve and explain the spatial and temporal observations of Fe-limitation in the CCE, with implications for global models of primary productivity and export.

## 5. Conclusions

Coastal filaments are seasonally transient features of high productivity in Eastern Boundary Upwelling Systems, connecting the coastal pelagic to the deep open ocean. The coastal upwelling filaments sampled allowed for in situ observation of developing Fe-limitation of diatom blooms carried offshore from areas of cool, nutrient-rich, upwelling waters. These are the first studies to follow coastal upwelling filaments in the CC from upwelling to offshore, in a Lagrangian fashion, with a focus on Fe biogeochemistry and Fe-limitation. We found that the extent to which $NO_3^-$ assimilation stimulated primary production in filaments depends on the availability of Fe. The BBL source of dFe is important, especially in the heavily Fe-limited MBF. The CUC is an additional new source of dFe and TDFe, which likely depends on the topography (headlands), latitude, and mixing at the mesoscale. Trends in this current suggest decreasing dissolved $O_2$ content (Evans et al., 2020; Ren et al., 2018). Ongoing climate change is expected to intensify regional droughts and ocean hypoxia which could have important consequences for Fe biogeochemistry in the CCE. We confirmed Fe-limitation occurs in upwelling filaments and this condition is reflected in macronutrients, upholding the use of geochemical proxies in the CCE. The development of Fe-limitation led to elevated in situ $NO_3^-$:dFe ratios and decreasing $Si_{ex}$ signatures. Deckboard incubation studies showed varying degrees of growth and uptake of $NO_3^-$ and $Si(OH)_4$ in response to Fe-fertilization in cycles located offshore from the continental shelf. Changes in the uptake ratios of the macronutrients and the effects of Fe-limitation on photosynthesis were linked to bSi:POC ratios of the phytoplankton communities. At Fe-limited stations, enhanced bSi:POC ratios are attributed to decreased POC content, rather than changes in bSi.

We presented evidence in support of enhanced organic carbon export efficiency offshore coincident with these biogeochemical spatial and temporal observations. In offshore evolutions of the filaments, we found enhanced export of carbon, which is in part a consequence of lateral transport of biogenic particles and enhanced ballasting of diatom communities due to increased bSi:POC ratios under Fe-limitation. This is an important step towards understanding how nutrients in mesoscale features in eastern boundary upwelling systems support high rates of primary production and facilitate carbon sequestration in the ocean. The length scales of macronutrients are related to incomplete utilization, which is modulated by Fe-limitation. Filaments are important for lateral advection of elements derived from the continental crust, as well as biogenic particulate matter, but dFe appears to be controlled by diatom community growth in the surface and water mass features and sediment plumes in the subsurface. We expect that a similar fate is shared for other bioactive or heavily scavenged metals derived from continental shelf sediments. The Lagrangian approach reveals that the *iron limitation mosaic* in the CCE is both *temporal* and *spatial*.

## Abbreviations

| | |
|---|---|
| AF | aged filament cycle |
| BBL | Benthic Boundary Layer |
| CCE | California Current Ecosystem |
| CUC | California Undercurrent |
| EF | early filament cycle |
| MBF | "Morro Bay" filament |
| Off | offshore cycle |
| PSF | "Pt. Sur" filament |
| Up | upwelling cycle |

## Data Availability Statement

CCE LTER data set variables generated in this study are dFe (https://doi.org/10.6073/pasta/50a0a46193bc6cbe7eaa1ba7510278e3; California Current Ecosystem LTER & Barbeau, 2023a), bSi (https://doi.org/10.6073/pasta/265091f2b7435d010e69ab27b7a0aa47; California Current Ecosystem LTER & Barbeau, 2023b), macronutrients (https://doi.org/10.6073/pasta/312e8060350f443b5e885ff33a2ddee8; California Current Ecosystem LTER and Goericke, 2022), POC (https://doi.org/10.6073/pasta/c1a975ce7bec5ee2b5bf7e10f9b9a8ac; California Current Ecosystem and Aluwihare, 2022), HPLC pigments (https://doi.org/10.6073/pasta/831e099fb086954d3d73638d33d3dd05; California Current Ecosystem LTER & Goericke, 2019), and hydrography (https://doi.org/10.6073/pasta/312e8060350f443b5e885ff33a2ddee8; California Current Ecosystem LTER and Goericke, 2022).

**Acknowledgments**

We thank CCE LTER and captains and crews of the *R/Vs Revelle* and *Atlantis* for facilitating sample collection, and chief scientist Mark Ohman for a visionary sampling plan as well as insightful input. Specifically, we thank Lauren Manck and Max Fenton for help with executing the trace element sampling plan. We also would like to thank Robert Sherrell, Vincent Roccanova, and Kaixan Bu for assistance with analyzing BBL samples for multiple trace elements and the Department of Marine and Coastal Sciences at Rutgers University. We are also grateful for Jack Pan (NASA JPL), Shonna Dovel, and Ralph Goericke at Scripps Institution of Oceanography for their expertise and assistance with the pigment data analysis. Data sets presented here were supported in part by CCE-LTER funding (NSF Grants OCE-1637632 and OCE-2224726). K.O.F. was supported by an NSF GRF (NSF 15-597). Sample analyses at Rutgers University were supported by an Edna Bailey Sussman Trust Special Merit Award in 2018.

## References

Ardiningsih, I., Krisch, S., Lodeiro, P., Reichart, G.-J., Achterberg, E. P., Gledhill, M., et al. (2020). Natural Fe-binding organic ligands in Fram Strait and over the northeast Greenland shelf. *Marine Chemistry*, *224*, 103815. https://doi.org/10.1016/j.marchem.2020.103815

Assmy, P., Smetacek, V., Montresor, M., Klaas, C., Henjes, J., Strass, V. H., et al. (2013). Thick-shelled, grazer-protected diatoms decouple ocean carbon and silicon cycles in the iron-limited Antarctic Circumpolar Current. *Proceedings of the National Academy of Sciences*, *110*(51), 20633–20638. https://doi.org/10.1073/pnas.1309345110

Barth, J. A., & Brink, K. H. (1987). Shipboard acoustic Doppler profiler velocity observations near Point Conception: Spring 1983. *Journal of Geophysical Research*, *92*(C4), 3925–3943. https://doi.org/10.1029/JC092iC04p03925

Biller, D. V., Coale, T. H., Till, R. C., Smith, G. J., & Bruland, K. W. (2013). Coastal iron and nitrate distributions during the spring and summer upwelling season in the central California Current upwelling regime. *Continental Shelf Research*, *66*, 58–72. https://doi.org/10.1016/j.csr.2013.07.003

Bograd, S. J., Schroeder, I. D., & Jacox, M. G. (2019). A water mass history of the Southern California current system. *Geophysical Research Letters*, *46*(12), 6690–6698. https://doi.org/10.1029/2019gl082685

Bourne, H. L., Bishop, J. K. B., Connors, E. J., & Wood, T. J. (2021). Carbon export and fate beneath a dynamic upwelled filament off the California coast. *Biogeosciences*, *18*(10), 3053–3086. https://doi.org/10.5194/bg-18-3053-2021

Boyle, E. A., Edmond, J. M., & Sholkovitz, E. R. (1977). The mechanism of iron removal in estuaries. *Geochimica et Cosmochimica Acta*, *41*(9), 1313–1324. https://doi.org/10.1016/0016-7037(77)90075-8

Bruland, K. W., Rue, E. L., & Smith, G. J. (2001). Iron and macronutrients in California coastal upwelling regimes: Implications for diatom blooms. *Limnology & Oceanography*, *46*(7), 1661–1674. https://doi.org/10.4319/lo.2001.46.7.1661

Bruland, K. W., Rue, E. L., Smith, G. J., & DiTullio, G. R. (2005). Iron, macronutrients and diatom blooms in the Peru upwelling regime: Brown and blue waters of Peru. *Marine Chemistry*, *93*(2), 81–103. https://doi.org/10.1016/j.marchem.2004.06.011

Brzezinski, M. A. (1985). The Si:C:N ratio of marine diatoms: Interspecific variability and the effect of some environmental variables 1. *Journal of Phycology*, *21*(3), 347–357. https://doi.org/10.1111/j.0022-3646.1985.00347.x

Brzezinski, M. A., Krause, J. W., Bundy, R. M., Barbeau, K. A., Franks, P., Goericke, R., et al. (2015). Enhanced silica ballasting from iron stress sustains carbon export in a frontal zone within the California Current. *Journal of Geophysical Research: Ocean*, *120*(7), 4654–4669. https://doi.org/10.1002/2015JC010829

Bundy, R. M., Biller, D. V., Buck, K. N., Bruland, K. W., & Barbeau, K. A. (2014). Distinct pools of dissolved iron-binding ligands in the surface and benthic boundary layer of the California Current. *Limnology & Oceanography*, *59*(3), 769–787. https://doi.org/10.4319/lo.2014.59.3.0769

Burdige, D. J., & Komada, T. (2020). Iron redox cycling, sediment resuspension and the role of sediments in low oxygen environments as sources of iron to the water column. *Marine Chemistry*, *223*, 103793. https://doi.org/10.1016/j.marchem.2020.103793

Burns, S. M., Bundy, R. M., Abbott, W., Abdala, Z., Sterling, A. R., Chappell, P. D., et al. (2023). Interactions of bioactive trace metals in shipboard Southern Ocean incubation experiments. *Limnology & Oceanography*, *68*(3), 525–543. https://doi.org/10.1002/lno.12290

California Current Ecosystem LTER, & Aluwihare, L. (2022). Particulate organic carbon and nitrogen measurements at selected depths in the water column in the CCE region since 2006 - 2019 (ongoing) ver 11. [Dataset]. Environmental Data Initiative. https://doi.org/10.6073/pasta/c1a975ce7bec5ee2b5bf7e10f9b9a8ac

California Current Ecosystem LTER, & Barbeau, K. (2023a). Measurements, from CCE LTER process cruises in the California Current region, of dissolved inorganic concentrations of nutrient iron and of iron limitation at selected stations and depths, 2006 - 2019 (ongoing) ver 6. [Dataset]. Environmental Data Initiative. https://doi.org/10.6073/pasta/50a0a46193bc6cbe7eaa1ba7510278e3

California Current Ecosystem LTER, & Barbeau, K. (2023b). Vertical profiles of in-situ biogenic silica (bSi) from discrete rosette bottle samples from CCE-LTER starting with cruise P1706 ver 2. [Dataset]. Environmental Data Initiative. https://doi.org/10.6073/pasta/265091f2b7435d010e69ab27b7a0aa47

California Current Ecosystem LTER, & Goericke, R. (2019). High Performance Liquid Chromatography (HPLC) pigment analysis from rosette bottle samples at various depths from CCE LTER process cruises in the California Current System, 2006 to 2017 ver 4. [Dataset]. Environmental Data Initiative. https://doi.org/10.6073/pasta/831e099fb086954d3d73638d33d3dd05

California Current Ecosystem LTER, & Goericke, R. (2022). Parameters from discrete bottle samples on a hydrographic CTD (Conductivity Temperature Depth) cast during CCE LTER process cruises in the CCE region, 2006 - 2019 (ongoing) ver 7. [Dataset]. Environmental Data Initiative. https://doi.org/10.6073/pasta/312e8060350f443b5e885ff33a2ddee8

Carr, M.-E. (2001). Estimation of potential productivity in Eastern Boundary Currents using remote sensing. *Deep Sea Research Part II: Topical Studies in Oceanography*, *49*(1), 59–80. https://doi.org/10.1016/S0967-0645(01)00094-7

Carr, M.-E., & Kearns, E. J. (2003). Production regimes in four Eastern Boundary Current systems. *Deep Sea Research Part II: Topical Studies in Oceanography*, *50*(22), 3199–3221. https://doi.org/10.1016/j.dsr2.2003.07.015

Centurioni, L. R., Ohlmann, J. C., & Niiler, P. P. (2008). Permanent Meanders in the California Current System. *Journal of Physical Oceanography*, *38*(8), 1690–1710. https://doi.org/10.1175/2008JPO3746.1

Chabert, P., d'Ovidio, F., Echevin, V., Stukel, M. R., & Ohman, M. D. (2021). Cross-shore flow and implications for carbon export in the California Current ecosystem: A Lagrangian analysis. *Journal of Geophysical Research: Ocean*, *126*(2), e2020JC016611. https://doi.org/10.1029/2020JC016611

Chase, Z., Hales, B., Cowles, T., Schwartz, R., & van Geen, A. (2005). Distribution and variability of iron input to Oregon coastal waters during the upwelling season. *Journal of Geophysical Research*, *110*(C10), C10S12. https://doi.org/10.1029/2004JC002590

Chase, Z., Strutton, P. G., & Hales, B. (2007). Iron links river runoff and shelf width to phytoplankton biomass along the U.S. West Coast, Geophys. *Res. Lett.*, *34*(4), L04607. https://doi.org/10.1029/2006GL028069

Chavez, F. P., Barber, R. T., Kosro, P. M., Huyer, A., Ramp, S. R., Stanton, T. P., & Rojas de Mendiola, B. (1991). Horizontal transport and the distribution of nutrients in the Coastal Transition Zone off northern California: Effects on primary production, phytoplankton biomass and species composition. *Journal of Geophysical Research*, *96*(C8), 14833–14848. https://doi.org/10.1029/91jc01163

Checkley, D. M., & Barth, J. A. (2009). Patterns and processes in the California Current System. *Progress in Oceanography*, *83*(1), 49–64. https://doi.org/10.1016/j.pocean.2009.07.028

Cutter, G. A., & Bruland, K. W. (2012). Rapid and noncontaminating sampling system for trace elements in global ocean surveys. *Limnology and Oceanography: Methods*, *10*(6), 425–436. https://doi.org/10.4319/lom.2012.10.425

Dale, A. W., Nickelsen, L., Scholz, F., Hensen, C., Oschlies, A., & Wallmann, K. (2015). A revised global estimate of dissolved iron fluxes from marine sediments. *Global Biogeochemical Cycles*, *29*(5), 691–707. https://doi.org/10.1002/2014GB005017

De La Rocha, C. L., Hutchins, D. A., Brzezinski, M. A., & Zhang, Y. (2000). Effects of iron and zinc deficiency on elemental composition and silica production by diatoms. *Marine Ecology Progress Series*, *195*, 71–79. [online]. https://doi.org/10.3354/meps195071

Dussin, R., Curchitser, E. N., Stock, C. A., & Van Oostende, N. (2019). Biogeochemical drivers of changing hypoxia in the California Current Ecosystem. *Deep Sea Research Part II: Topical Studies in Oceanography*, *169–170*, 104590. https://doi.org/10.1016/j.dsr2.2019.05.013

Elrod, V. A., Berelson, W. M., Coale, K. H., & Johnson, K. S. (2004). The flux of iron from continental shelf sediments: A missing source for global budgets. *Geophysical Research Letters*, *31*(12), L12307. https://doi.org/10.1029/2004GL020216

Evans, N., Schroeder, I. D., Pozo Buil, M., Jacox, M. G., & Bograd, S. J. (2020). Drivers of subsurface deoxygenation in the southern California Current System. *Geophysical Research Letters*, *47*(21), e2020GL089274. https://doi.org/10.1029/2020GL089274

Field, C. B., Behrenfeld, M. J., Randerson, J. T., & Falkowski, P. (1998). Primary production of the biosphere: Integrating terrestrial and oceanic components. *Science*, *281*(5374), 237–240. https://doi.org/10.1126/science.281.5374.237

Firme, G. F., Rue, E. L., Weeks, D. A., Bruland, K. W., & Hutchins, D. A. (2003). Spatial and temporal variability in phytoplankton iron limitation along the California coast and consequences for Si, N, and C biogeochemistry. *Global Biogeochemical Cycles*, *17*(1), 1016. https://doi.org/10.1029/2001GB001824

Franck, V. M., Bruland, K. W., Hutchins, D. A., & Brzezinski, M. (2003). Iron and zinc effects on silicic acid and nitrate uptake kinetics in three high-nutrient, low-chlorophyll (HNLC) regions. *Marine Ecology Progress Series*, *252*, 15–33. [online]. https://doi.org/10.3354/meps252015

Franck, V. M., Brzezinski, M. A., Coale, K. H., & Nelson, D. M. (2000). Iron and silicic acid concentrations regulate Si uptake north and south of the Polar Frontal Zone in the Pacific Sector of the Southern Ocean. *Deep Sea Research Part II: Topical Studies in Oceanography*, *47*(15), 3315–3338. https://doi.org/10.1016/S0967-0645(00)00070-9

Gangrade, S., & Franks, P. J. S. (2023). Phytoplankton patches at oceanic fronts are linked to coastal upwelling pulses: Observations and implications in the California Current System. *Journal of Geophysical Research: Ocean*, *128*(3), e2022JC019095. https://doi.org/10.1029/2022JC019095

Hickey, B. M. (1998). Coastal oceanography of western North American from the tip of Baja California to Vancouver Island, Coastal Segment (8, E). *The Sea*, *11*, 345–393. Retrieved from https://cir.nii.ac.jp/crid/1572543025329871488.bib?lang=en

Hoffmann, L. J., Peeken, I., & Lochte, K. (2007). Effects of iron on the elemental stoichiometry during EIFEX and in the diatoms Fragilariopsis kerguelensis and Chaetoceros dichaeta. *Biogeosciences*, *4*(4), 569–579. https://doi.org/10.5194/bg-4-569-2007

Hogle, S. L., Dupont, C. L., Hopkinson, B. M., King, A. L., Buck, K. N., Roe, K. L., et al. (2018). Pervasive iron limitation at subsurface chlorophyll maxima of the California Current. *Proceedings of the National Academy of Sciences*, *115*(52), 13300–13305. https://doi.org/10.1073/pnas.1813192115

Homoky, W. B., Severmann, S., McManus, J., Berelson, W. M., Riedel, T. E., Statham, P. J., & Mills, R. A. (2012). Dissolved oxygen and suspended particles regulate the benthic flux of iron from continental margins. *Marine Chemistry*, *134*(Supplement C), 59–70. https://doi.org/10.1016/j.marchem.2012.03.003

Hopwood, M. J., Carroll, D., Dunse, T., Hodson, A., Holding, J. M., Iriarte, J. L., et al. (2020). Review article: How does glacier discharge affect marine biogeochemistry and primary production in the Arctic? *The Cryosphere*, *14*(4), 1347–1383. https://doi.org/10.5194/tc-14-1347-2020

Hutchins, D. A., & Bruland, K. W. (1998). Iron-limited diatom growth and Si:N uptake ratios in a coastal upwelling regime. *Nature*, *393*(6685), 561–564. https://doi.org/10.1038/31203

Hutchins, D. A., DiTullio, G. R., Zhang, Y., & Bruland, K. W. (1998). An iron limitation mosaic in the California upwelling regime. *Limnology & Oceanography*, *43*(6), 1037–1054. https://doi.org/10.4319/lo.1998.43.6.1037

Hutchins, D. A., Hare, C. E., Weaver, R. S., Zhang, Y., Firme, G. F., DiTullio, G. R., et al. (2002). Phytoplankton iron limitation in the Humboldt Current and Peru Upwelling. *Limnology & Oceanography*, *47*(4), 997–1011. https://doi.org/10.4319/lo.2002.47.4.0997

Johnson, K. S., Chavez, F. P., & Friederich, G. E. (1999). Continental-shelf sediment as a primary source of iron for coastal phytoplankton. *Nature*, *398*(6729), 697–700. https://doi.org/10.1038/19511

Kelly, T. B., Goericke, R., Kahru, M., Song, H., & Stukel, M. R. (2018). CCE II: Spatial and interannual variability in export efficiency and the biological pump in an eastern boundary current upwelling system with substantial lateral advection. *Deep Sea Research Part I: Oceanographic Research Papers*, *140*, 14–25. https://doi.org/10.1016/j.dsr.2018.08.007

Kim, S. Y., Terrill, E. J., Cornuelle, B. D., Jones, B., Washburn, L., Moline, M. A., et al. (2011). Mapping the U.S. West Coast surface circulation: A multiyear analysis of high-frequency radar observations. *Journal of Geophysical Research*, *116*(C3), C03011. https://doi.org/10.1029/2010JC006669

King, A. L., & Barbeau, K. A. (2007). Evidence for phytoplankton iron limitation in the southern California Current System. *Marine Ecology Progress Series*, *342*, 91–103. https://doi.org/10.3354/meps342091

King, A. L., & Barbeau, K. A. (2011). Dissolved iron and macronutrient distributions in the southern California Current System. *Journal of Geophysical Research*, *116*(C3), C03018. https://doi.org/10.1029/2010JC006324

Knauer, G. A., Martin, J. H., & Bruland, K. W. (1979). Fluxes of particulate carbon, nitrogen, and phosphorus in the upper water column of the northeast Pacific. *Deep Sea Research Part A: Oceanographic Research Papers*, *26*(1), 97–108. https://doi.org/10.1016/0198-0149(79)90089-X

Kranz, S. A., Wang, S., Kelly, T. B., Stukel, M. R., Goericke, R., Landry, M. R., & Cassar, N. (2020). Lagrangian studies of marine production: A multimethod assessment of productivity relationships in the California Current ecosystem upwelling region. *Journal of Geophysical Research: Ocean*, *125*(6), e2019JC015984. https://doi.org/10.1029/2019JC015984

Krause, J. W., Brzezinski, M. A., Goericke, R., Landry, M. R., Ohman, M. D., Stukel, M. R., & Taylor, A. G. (2015). Variability in diatom contributions to biomass, organic matter production and export across a frontal gradient in the California Current Ecosystem. *Journal of Geophysical Research: Ocean*, *120*(2), 1032–1047. https://doi.org/10.1002/2014JC010472

Krause, J. W., Brzezinski, M. A., Largier, J. L., McNair, H. M., Maniscalco, M., Bidle, K. D., et al. (2020). The interaction of physical and biological factors drives phytoplankton spatial distribution in the northern California Current. *Limnology & Oceanography*, *65*(9), 1974–1989. https://doi.org/10.1002/lno.11431

Kurczyn, J. A., Pérez-Brunius, P., López, M., Candela, J., Delgadillo-Hinojosa, F., & García-Mendoza, E. (2019). Water masses and ocean currents over the continental slope off northern Baja California. *Journal of Geophysical Research: Ocean*, *124*(4), 2803–2823. https://doi.org/10.1029/2018JC013962

Lam, P. J., Lee, J.-M., Heller, M. I., Mehic, S., Xiang, Y., & Bates, N. R. (2018). Size-fractionated distributions of suspended particle concentration and major phase composition from the U.S. GEOTRACES Eastern Pacific Zonal Transect (GP16). *Marine Chemistry*, *201*, 90–107. https://doi.org/10.1016/j.marchem.2017.08.013

Landry, M. R., Ohman, M. D., Goericke, R., Stukel, M. R., & Tsyrklevich, K. (2009). Lagrangian studies of phytoplankton growth and grazing relationships in a coastal upwelling ecosystem off Southern California. *Progress in Oceanography*, *83*(1), 208–216. https://doi.org/10.1016/j.pocean.2009.07.026

Longhurst, A. R., & Glen Harrison, W. (1989). The biological pump: Profiles of plankton production and consumption in the upper ocean. *Progress in Oceanography*, *22*(1), 47–123. https://doi.org/10.1016/0079-6611(89)90010-4

Marchetti, A., & Cassar, N. (2009). Diatom elemental and morphological changes in response to iron limitation: A brief review with potential paleoceanographic applications. *Geobiology*, *7*(4), 419–431. https://doi.org/10.1111/j.1472-4669.2009.00207.x

Marchetti, A., & Harrison, P. J. (2007). Coupled changes in the cell morphology and elemental (C, N, and Si) composition of the pennate diatom Pseudo-nitzschia due to iron deficiency. *Limnology & Oceanography*, *52*(5), 2270–2284. https://doi.org/10.4319/lo.2007.52.5.2270

Marchetti, A., Maldonado, M. T., Lane, E. S., & Harrison, P. J. (2006). Iron requirements of the pennate diatom Pseudo-nitzschia: Comparison of oceanic (high-nitrate, low-chlorophyll waters) and coastal species. *Limnology & Oceanography*, *51*(5), 2092–2101. https://doi.org/10.4319/lo.2006.51.5.2092

Milne, A., Schlosser, C., Wake, B. D., Achterberg, E. P., Chance, R., Baker, A. R., et al. (2017). Particulate phases are key in controlling dissolved iron concentrations in the (sub)tropical North Atlantic. *Geophysical Research Letters*, *44*(5), 2377–2387. https://doi.org/10.1002/2016GL072314

Mohrholz, V., Eggert, A., Junker, T., Nausch, G., Ohde, T., & Schmidt, M. (2014). Cross shelf hydrographic and hydrochemical conditions and their short term variability at the northern Benguela during a normal upwelling season. *Journal of Marine Systems*, *140*, 92–110. https://doi.org/10.1016/j.jmarsys.2014.04.019

Morel, F. M. M. (2008). The co-evolution of phytoplankton and trace element cycles in the oceans. *Geobiology*, *6*(3), 318–324. https://doi.org/10.1111/j.1472-4669.2008.00144.x

Morrow, R. M., Ohman, M. D., Goericke, R., Kelly, T. B., Stephens, B. M., Stukel, M. R., & CCE, V. (2018). Primary production, mesozooplankton grazing, and the biological pump in the California Current Ecosystem: Variability and response to El Niño. *Deep Sea Research Part I: Oceanographic Research Papers*, *140*, 52–62. https://doi.org/10.1016/j.dsr.2018.07.012

Muller, A. A., Mohrholz, V., & Schmidt, M. (2013). The circulation dynamics associated with a northern Benguela upwelling filament during October 2010. *Continental Shelf Research*, *63*, 59–68. https://doi.org/10.1016/j.csr.2013.04.037

Nagai, T., Gruber, N., Frenzel, H., Lachkar, Z., McWilliams, J. C., & Plattner, G.-K. (2015). Dominant role of eddies and filaments in the offshore transport of carbon and nutrients in the California Current System. *Journal of Geophysical Research: Ocean*, *120*(8), 5318–5341. https://doi.org/10.1002/2015JC010889

Nelson, D. M., Tréguer, P., Brzezinski, M. A., Leynaert, A., & Quéguiner, B. (1995). Production and dissolution of biogenic silica in the ocean: Revised global estimates, comparison with regional data and relationship to biogenic sedimentation. *Global Biogeochemical Cycles*, *9*(3), 359–372. https://doi.org/10.1029/95GB01070

Plattner, G.-K., Gruber, N., Frenzel, H., & McWilliams, J. C. (2005). Decoupling marine export production from new production. *Geophysical Research Letters*, *32*(11), L11612. https://doi.org/10.1029/2005GL022660

Price, N. M. (2005). The elemental stoichiometry and composition of an iron-limited diatom. *Limnology & Oceanography*, *50*(4), 1159–1171. https://doi.org/10.4319/lo.2005.50.4.1159

Quéguiner, B. (2013). Iron fertilization and the structure of planktonic communities in high nutrient regions of the Southern Ocean. *Deep Sea Research Part II: Topical Studies in Oceanography*, *90*, 43–54. https://doi.org/10.1016/j.dsr2.2012.07.024

Rafter, P. A., Sigman, D. M., & Mackey, K. R. M. (2017). Recycled iron fuels new production in the eastern equatorial Pacific Ocean. *Nature Communications*, *8*(1), 1100. https://doi.org/10.1038/s41467-017-01219-7

Ren, A. S., Chai, F., Xue, H., Anderson, D. M., & Chavez, F. P. (2018). A sixteen-year decline in dissolved oxygen in the central California Current. *Scientific Reports*, *8*(1), 7290. https://doi.org/10.1038/s41598-018-25341-8

Rossi, V., Garçon, V., Tassel, J., Romagnan, J.-B., Stemmann, L., Jourdin, F., et al. (2013). Cross-shelf variability in the Iberian Peninsula Upwelling System: Impact of a mesoscale filament. *Continental Shelf Research*, *59*, 97–114. https://doi.org/10.1016/j.csr.2013.04.008

Rudnick, D. L., Zaba, K. D., Todd, R. E., & Davis, R. E. (2017). A climatology of the California Current System from a network of underwater gliders. *Progress in Oceanography*, *154*, 64–106. https://doi.org/10.1016/j.pocean.2017.03.002

Sangrà, P., Troupin, C., Barreiro-González, B., Desmond Barton, E., Orbi, A., & Arístegui, J. (2015). The Cape Ghir filament system in August 2009 (NW Africa). *Journal of Geophysical Research: Ocean*, *120*(6), 4516–4533. https://doi.org/10.1002/2014JC010514

Sedwick, P. N., DiTullio, G. R., & Mackey, D. J. (2000). Iron and manganese in the Ross Sea, Antarctica: Seasonal iron limitation in Antarctic shelf waters. *Journal of Geophysical Research*, *105*(C5), 11321–11336. https://doi.org/10.1029/2000JC000256

Sherrell, R. M., Annett, A. L., Fitzsimmons, J. N., Roccanova, V. J., & Meredith, M. P. (2018). A "shallow bathtub ring" of local sedimentary iron input maintains the Palmer Deep biological hotspot on the West Antarctic Peninsula shelf. *Philosophical Transactions of the Royal Society A: Mathematical, Physical and Engineering Sciences*, *376*(2122), 20170171. https://doi.org/10.1098/rsta.2017.0171

Smetacek, V. (1999). Diatoms and the ocean carbon cycle. *Protist*, *150*(1), 25–32. https://doi.org/10.1016/S1434-4610(99)70006-4

Smith, S. R., Gillard, J. T. F., Kustka, A. B., McCrow, J. P., Badger, J. H., Zheng, H., et al. (2016). Transcriptional orchestration of the global cellular response of a model pennate diatom to diel light cycling under iron limitation. *PLoS Genetics*, *12*(12), e1006490. [online]. https://doi.org/10.1371/journal.pgen.1006490

Stukel, M. R., Aluwihare, L. I., Barbeau, K. A., Chekalyuk, A. M., Goericke, R., Miller, A. J., et al. (2017). Mesoscale ocean fronts enhance carbon export due to gravitational sinking and subduction. *Proceedings of the National Academy of Sciences*, *114*(6), 1252–1257. https://doi.org/10.1073/pnas.1609435114

Stukel, M. R., & Barbeau, K. A. (2020). Investigating the nutrient landscape in a coastal upwelling region and its relationship to the biological carbon pump. *Geophysical Research Letters*, *47*(6), e2020GL087351. https://doi.org/10.1029/2020GL087351

Sverdrup, H. (1938). Oceanographic problems off the coast of California. *Eos, Transactions, American Geophysical Union*, *19*(1), 173–174. https://doi.org/10.1029/tr019i001p00173

Takeda, S. (1998). Influence of iron availability on nutrient consumption ratio of diatoms in oceanic waters. *Nature*, *393*(6687), 774–777. https://doi.org/10.1038/31674

Till, C. P., Solomon, J. R., Cohen, N. R., Lampe, R. H., Marchetti, A., Coale, T. H., & Bruland, K. W. (2019). The iron limitation mosaic in the California Current System: Factors governing Fe availability in the shelf/near-shelf region. *Limnology & Oceanography*, *64*(1), 109–123. https://doi.org/10.1002/lno.11022

Timmermans, K. R., van der Wagt, B., & de Baar, H. J. W. (2004). Growth rates, half-saturation constants, and silicate, nitrate, and phosphate depletion in relation to iron availability of four large, open-ocean diatoms from the Southern Ocean. *Limnology & Oceanography*, *49*(6), 2141–2151. https://doi.org/10.4319/lo.2004.49.6.2141

Tréguer, P., Bowler, C., Moriceau, B., Dutkiewicz, S., Gehlen, M., Aumont, O., et al. (2018). Influence of diatom diversity on the ocean biological carbon pump. *Nature Geoscience*, *11*(1), 27–37. https://doi.org/10.1038/s41561-017-0028-x

Twining, B. S., Antipova, O., Chappell, P. D., Cohen, N. R., Jacquot, J. E., Mann, E. L., et al. (2021). Taxonomic and nutrient controls on phytoplankton iron quotas in the ocean. *Limnology and Oceanography Letters*, *6*(2), 96–106. https://doi.org/10.1002/lol2.10179

Twining, B. S., Baines, S. B., & Fisher, N. S. (2004). Element stoichiometries of individual plankton cells collected during the Southern Ocean Iron Experiment (SOFeX). *Limnology & Oceanography*, *49*(6), 2115–2128. https://doi.org/10.4319/lo.2004.49.6.2115

Van Oostende, N., Dunne, J. P., Fawcett, S. E., & Ward, B. B. (2015). Phytoplankton succession explains size-partitioning of new production following upwelling-induced blooms. *Journal of Marine Systems*, *148*, 14–25. https://doi.org/10.1016/j.jmarsys.2015.01.009

Wang, S., Kranz, S. A., Kelly, T. B., Song, H., Stukel, M. R., & Cassar, N. (2020). Lagrangian studies of Net community production: The effect of diel and multiday nonsteady state factors and vertical fluxes on O2/Ar in a dynamic upwelling region. *Journal of Geophysical Research: Biogeosciences*, *125*(6), e2019JG005569. https://doi.org/10.1029/2019JG005569

White, M. E., Rafter, P. A., Stephens, B. M., Mazloff, M. R., Wankel, S. D., & Aluwihare, L. I. (2022). Stable isotopes of nitrate record effects of the 2015–2016 El Niño and diatom iron limitation on nitrogen cycling in the eastern North Pacific Ocean. *Limnology & Oceanography*, *67*(10), 2140–2156. https://doi.org/10.1002/lno.12194

Wilken, S., Hoffmann, B., Hersch, N., Kirchgessner, N., Dieluweit, S., Rubner, W., et al. (2011). Diatom frustules show increased mechanical strength and altered valve morphology under iron limitation. *Limnology & Oceanography*, *56*(4), 1399–1410. https://doi.org/10.4319/lo.2011.56.4.1399

Winant, C. D., Alden, D. J., Dever, E. P., Edwards, K. A., & Hendershott, M. C. (1999). Near-surface trajectories off central and southern California. *Journal of Geophysical Research*, *104*(C7), 15713–15726. https://doi.org/10.1029/1999JC900083

Winant, C. D., Dever, E. P., & Hendershott, M. C. (2003). Characteristic patterns of shelf circulation at the boundary between central and southern California. *Journal of Geophysical Research*, *108*(C2), 3021. https://doi.org/10.1029/2001JC001302

Zaba, K. D., Franks, P. J. S., & Ohman, M. D. (2021). The California Undercurrent as a source of upwelled waters in a coastal filament. *Journal of Geophysical Research: Ocean*, *126*(2), e2020JC016602. https://doi.org/10.1029/2020JC016602

Zentara, S. J., & Kamykowski, D. (1977). Latitudinal relationships among temperature and selected plant nutrients along the west coast of North and South America. *Journal of Marine Research*, *35*(2), 321–337.

Zhang, S., Liu, H., Ke, Y., & Li, B. (2017). Effect of the silica content of diatoms on protozoan grazing. *Frontiers in Marine Science*, *4*, 202. [online]. https://doi.org/10.3389/fmars.2017.00202

## References From the Supporting Information

Brzezinski, M. A., & Nelson, D. M. (1995). The annual silica cycle in the Sargasso Sea near Bermuda. *Deep Sea Research Part I: Oceanographic Research Papers*, *42*(7), 1215–1237. https://doi.org/10.1016/0967-0637(95)93592-3

Forsch, K., Hahn-Woernle, L., Sherrell, R., Roccanova, J., Bu, K., Burdige, D., et al. (2021). Seasonal dispersal of fjord meltwaters as an important source of iron to coastal Antarctic phytoplankton. *Biogeosciences Discussions*, *2021*, 1–49. https://doi.org/10.5194/bg-2021-79

Frenger, I., Bianchi, D., Stührenberg, C., Oschlies, A., Dunne, J., Deutsch, C., et al. (2018). Biogeochemical role of subsurface coherent eddies in the ocean: Tracer cannonballs, hypoxic storms, and microbial stewpots? *Global Biogeochemical Cycles*, *32*(2), 226–249. https://doi.org/10.1002/2017GB005743

González-Silvera, A., Santamaría-del-Ángel, E., Camacho-Ibar, V., López-Calderón, J., Santander-Cruz, J., & Mercado-Santana, A. (2020). The effect of cold and warm anomalies on phytoplankton pigment composition in waters off the northern Baja California Peninsula (México): 2007–2016. *Journal of Marine Science and Engineering*, *8*(7), 533. https://doi.org/10.3390/jmse8070533

Lohan, M. C., Aguilar-Islas, A. M., & Bruland, K. W. (2006). Direct determination of iron in acidified (pH 1.7) seawater samples by flow injection analysis with catalytic spectrophotometric detection: Application and intercomparison. *Limnology and Oceanography: Methods*, *4*(6), 164–171. https://doi.org/10.4319/lom.2006.4.164

Lukas, R., & Santiago-Mandujano, F. (2001). Extreme water mass anomaly observed in the Hawaii ocean time-series. *Geophysical Research Letters*, *28*(15), 2931–2934. https://doi.org/10.1029/2001GL013099

Strickland, J. D. H., & Parsons, T. R. (1972). *A practical handbook of seawater analysis*. Fisheries Research Board of Canada